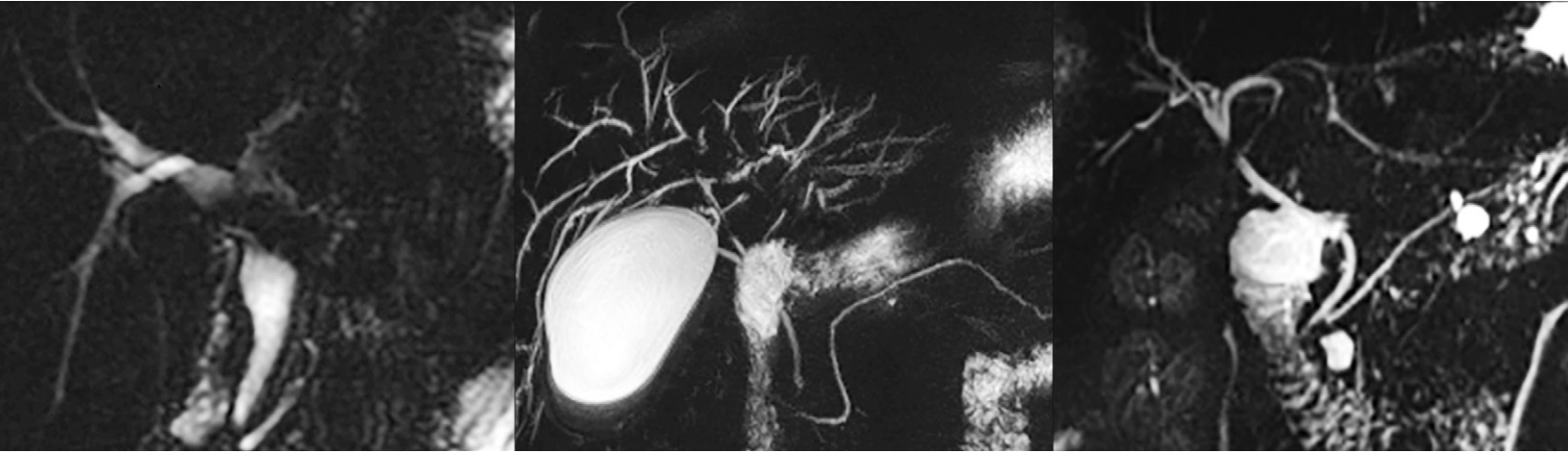


Imaging of Biliary Tree Abnormalities

Camila Lopes Vendrami, MD* • Deanna L. Thorson, MD* • Amir A. Borhani, MD • Pardeep K. Mittal, MD • Nancy A. Hammond, MD • David J. Escobar, MD
Helena Gabriel, MD • Hannah S. Recht, MD • Jeanne M. Horowitz, MD • Linda C. Kelahan, MD • Cecil G. Wood, MD • Paul Nikolaidis, MD
Sudhakar K. Venkatesh, MD • Frank H. Miller, MD

* C.L.V. and D.L.T. contributed equally to this work.
Author affiliations, funding, and conflicts of interest are listed at [the end of this article](#).



Pathologic conditions of the biliary system, although common, can be difficult to diagnose clinically. Challenges in biliary imaging include anatomic variants and the dynamic nature of the biliary tract, which can change with age and intervention, blurring the boundaries of normal and abnormal. Choledochal cysts can have numerous appearances and are important to diagnose given the risk of cholangiocarcinoma potentially requiring surgical resection. Choledocholithiasis, the most common cause of biliary dilatation, can be difficult to detect at US and CT, with MRI having the highest sensitivity. However, knowledge of the imaging pitfalls of MRI and MR cholangiopancreatography is crucial to avoid misinterpretation. Newer concepts in biliary tract malignancy include intraductal papillary biliary neoplasms that may develop into cholangiocarcinoma. New paradigms in the classification of cholangiocarcinoma correspond to the wide range of imaging appearances of the disease and have implications for prognosis. Accurately staging cholangiocarcinoma is imperative, given expanding curative options including transplant and more aggressive surgical options. Infections of the biliary tree include acute cholangitis or recurrent pyogenic cholangitis, characterized by obstruction, strictures, and central biliary dilatation. Inflammatory conditions include primary sclerosing cholangitis, which features strictures and fibrosis but can be difficult to differentiate from secondary causes of sclerosing cholangitis, including more recently described entities such as immunoglobulin G4-related sclerosing cholangitis and COVID-19 secondary sclerosing cholangitis. The authors describe a wide variety of benign and malignant biliary tract abnormalities, highlight differentiating features of the cholangitides, provide an approach to interpretation based on the pattern of imaging findings, and discuss pearls and pitfalls of imaging to facilitate accurate diagnosis.

©RSNA, 2024 • radiographics.rsna.org

Introduction

Radiologists' interpretation of noninvasive imaging of the biliary tree provides crucial guidance for multidisciplinary management of pathologic conditions of the biliary system. Imaging with US, CT, MRI, or MR cholangiopancreatography (MRCP) is frequently used for diagnosis before biliary procedures are performed by interventional radiologists, interventional gastroenterologists, or pancreaticobiliary surgeons. In addition, because clinical and histopathologic diagnosis of biliary entities can be challenging, radiologic findings contribute sub-

stantially to accurate diagnosis. Diagnosing biliary disease at imaging requires differentiation of a true biliary abnormality from artifacts and other imaging pitfalls, in addition to familiarity with the imaging appearance of a wide variety of biliary abnormalities. On recognition of the presence of a bile duct abnormality, evaluation of the most prominent imaging feature (luminal dilatation or narrowing, filling defects, wall thickening, or masses) with a pattern-based approach helps to guide the differential diagnosis. In this article, the authors provide a review of a variety of biliary tract diseases, with a focus on the

Supplemental
MaterialTest Your
Knowledge

RadioGraphics 2024; 44(8):e230174
<https://doi.org/10.1148/rg.230174>

Content Codes: CT, GI, MR

Abbreviations: ERCP = endoscopic retrograde cholangiopancreatography, IgG4 = immunoglobulin G4, IPNB = intraductal papillary mucinous neoplasm of the bile ducts, MIP = maximum intensity projection, MRCP = MR cholangiopancreatography, PSC = primary sclerosing cholangitis

TEACHING POINTS

- Intrahepatic and common bile duct stones (usually T1-hyperintense pigment stones at MRCP) without gallstones should prompt evaluation for causes of chronic biliary stasis including recurrent pyogenic cholangitis, PSC, or Caroli disease.
- A progressively enhancing perihilar mass, an intraductal luminal mass, or focal periductal soft-tissue thickening with delayed enhancement or vascular narrowing encountered in a patient with PSC is highly suggestive of cholangiocarcinoma. Identification of a high-grade stricture is also suspicious and warrants ERCP, particularly if it is associated with periductal thickening or worsening lobar atrophy.
- On biliary images, IgG4 sclerosing cholangitis may mimic other forms of cholangitis, especially PSC, but characteristic multiorgan involvement including pancreatic, renal, and salivary gland involvement and retroperitoneal fibrosis provide a diagnostic clue.
- Although MRCP is the ideal imaging modality for choledocholithiasis, it is important to not rely solely on the maximum intensity projection (MIP) images, which can obscure small filling defects, but to assess the source and thin-section T2-weighted MR images for stones.
- In comparison to benign strictures, malignant strictures often demonstrate irregular luminal narrowing with an abrupt transition in caliber and shouldered edges. Asymmetric ductal wall thickening, especially that greater than 3 mm, is suggestive of malignant stricture.

salient key features that help radiologists to differentiate these pathologic conditions with noninvasive imaging, when possible, and to guide management when a specific diagnosis cannot be determined from imaging alone.

Normal Biliary Anatomy and Variants

The normal anatomy of the biliary system, present in 58% of the population, consists of the left and right hepatic ducts joining to form the common hepatic duct, which then joins the cystic duct to become the common bile duct. The right hepatic duct has two major branches: the right posterior duct (draining hepatic segments VI and VII) and the right anterior duct (draining hepatic segments V and VIII). The right posterior duct usually joins the right anterior duct from a medial (left) approach to form the right hepatic duct. The left hepatic duct is formed by union of the segment II, III, IVa, and IVb ducts. The caudate lobe bile duct can join the origin of either the left or right hepatic duct. There are several common anatomic variants of the biliary system (Table 1) (1). The extrahepatic duct drains into the ampulla of Vater, usually at the second (75%) or third portion of the duodenum (2).

A normal diameter of the extrahepatic duct (referring to both the common hepatic and common bile ducts) is generally considered to be 6 mm at its most distended segment when measured from the inner wall to the inner wall perpendicular to the course of the duct on images from any modality

in most patients younger than 60 years old. Intrahepatic duct dilatation is defined as greater than 2 mm or greater than 40% of the width of its corresponding portal vein (3). In patients older than 60 years, 8 mm is thought to be a more reliable threshold for a normal common duct diameter (3). In patients who have undergone cholecystectomy, an extrahepatic duct diameter up to 10 mm may be normal (3). Opioid use, especially use of morphine, has been cited as an additional cause of nonobstructive biliary dilatation (4).

Choledochal Cysts

Choledochal cysts are not actually conventional cysts, but malformations resulting in duct dilatation. They can predispose patients to cholestasis, choledocholithiasis, cholangitis, pancreatitis, and malignancy. There are multiple subtypes of choledochal malformations classified by the popular Todani classification system (Figs 1, 2) and, more recently, the Vissler classification system (Table 2) (5,6). The main differences between these classification systems is that the Visser classification system separates the categories of choledochal cysts by proposed cause and management protocols (and names the subtypes), whereas the Todani system uses Roman numerals to label and group subtypes. This can cause confusion in diagnosis and treatment because it suggests that these subtypes are related. The causes of these malformations are not definitely known, but several mechanisms including congenital anomaly have been proposed (Table 2) (5,6). Isolated dilatation of the cystic duct is referred to as a “type VI choledochal cyst” but is rare (7).

Choledochal cysts are usually diagnosed in childhood, but 20% are identified in adulthood (6,8). They are frequently detected with US, but MRCP is the optimal modality to evaluate the extent of involvement and the pancreaticobiliary junction. Pancreaticobiliary maljunction can be recognized as early extrahepatic union of the common bile and pancreatic ducts, usually resulting in a common channel measuring more than 1 cm in length (Fig S1) (8,9). Hepatobiliary MRI contrast agents can confirm communication of saccular cysts with the biliary tree (Fig 3), helping to exclude other lesions such as mucinous cystic neoplasms (9).

Surgical resection is the definitive treatment of most extrahepatic choledochal cysts, while segmentectomy or transplant may be undertaken for intrahepatic involvement (6). Postsurgical imaging surveillance is warranted because resection reduces but does not eliminate the risk of cholangiocarcinoma in patients with choledochal cysts (recently estimated at 3%–5% incidence) (6,10). A proposed mechanism of carcinogenesis is abnormal exposure of the biliary epithelium to pancreatic enzymes, which may account for cholangiocarcinoma developing in the extrahepatic duct of type I or type IV cysts (6,10).

Caroli disease (ie, type V choledochal cyst) is an autosomal recessive condition of ductal plate malformation affecting the large intrahepatic ducts, resulting in multifocal saccular dilatation of the intrahepatic ducts. “Caroli syndrome” refers to Caroli disease coexisting with congenital hepatic fibrosis due to abnormal formation of the small intrahepatic ducts and can also be associated with polycystic kidney

Table 1: Description and Incidence of Biliary Anatomic Variants

| Type of Variant | Percentage of the Population |
|---|------------------------------|
| Biliary anatomic variants | |
| Right posterior duct to left hepatic duct | 13–19 |
| Right posterior duct joining the right aspect of the right anterior duct | 12 |
| Confluence of right posterior, right anterior, and left hepatic ducts (triple confluence) | 11 |
| Right posterior duct drainage to common hepatic duct | 0–5 |
| Accessory hepatic ducts | 2 |
| Cystic variants | |
| Medial (left) cystic duct insertion | 10–17 |
| Low cystic duct joining the distal one-third of the common hepatic duct | 9 |
| Parallel course of the cystic duct (2-cm length or longer) | 1.5–25 |

Source.—Reference 1.

Note.—Uncommon variants include high cystic duct insertion to the common hepatic duct, insertion of the cystic duct with the right or left hepatic duct, and fusion of the right posterior and cystic ducts.

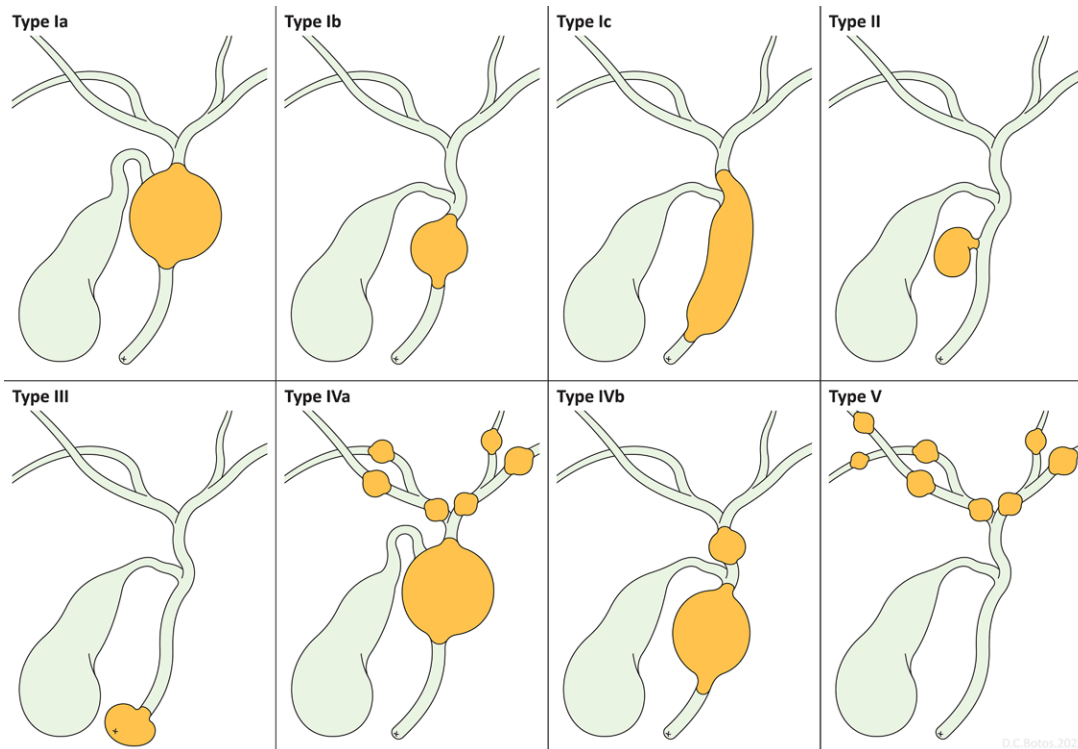


Figure 1. Illustrations show the Todani classification system for choledochal cysts. Type I cysts (the most common morphology) show dilatation of the extrahepatic bile duct. Type Ia cysts show cystic dilatation of the extrahepatic bile duct, with an abnormal pancreaticobiliary junction (not pictured). Type Ib cysts show focal dilatation of the common bile duct, without an abnormal pancreaticobiliary junction. Type Ic cysts show fusiform dilatation involving the common hepatic and common bile duct with an abnormal pancreaticobiliary junction. Type II cysts are diverticula of the supra-duodenal extrahepatic duct, usually projecting to the right. Type III cysts (ie, choledochoceles) show cystic dilatation of the intramural segment of the distal common bile duct protruding into the duodenum. Type IV cysts consist of multiple foci of dilatation, often with an abnormal pancreaticobiliary junction and involving either intrahepatic and extrahepatic ducts (IVa) or extrahepatic ducts alone (IVb). Type V cysts (ie, Caroli disease) are characterized by multiple intrahepatic cysts, without extrahepatic abnormality.



Figure 2. Todani type IVb choledochal cyst. Coronal maximum intensity projection (MIP) MRCP image shows a type IVb choledochal cyst with fusiform dilatation of the extrahepatic duct (short arrow) and a choledochoceles in the duodenal wall (long arrow). Type IVb choledochal cysts demonstrate multiple foci of extrahepatic ductal dilatation, without intrahepatic involvement. Multifocal dilatation can but is not required to include a choledochoceles.

Table 2: Todani vs Visser Classification of Choledochochal Cysts

| Todani Classification | | Visser Classification | | |
|-----------------------|--|------------------------------|---|--|
| Type | Details | Name | Details | Proposed Causes |
| I | Extrahepatic duct dilatation: 1a: diffuse cystic 1b: focal cystic 1c: diffuse fusiform | Congenital choledochal cysts | Todani types I and IV are combined as a spectrum of extrahepatic dilatation with varying intrahepatic involvement | 90% of cases: related to common channel syndrome 10% of cases: primary biliary strictures, ganglion cell insufficiency, abnormal congenital recanalization, and reovirus infection |
| II | Supraduodenal extrahepatic diverticulum | Choledochal diverticulum | A true diverticulum lined with biliary epithelium | Dysfunction of the sphincter of Oddi |
| III | Choledochoceles of the intraduodenal portion of the extrahepatic duct | Choledochoceles | Dilated segment of extrahepatic duct prolapsing into duodenum | Scarring or inflammation after passage of calculi |
| IV | Multifocal duct dilatation: IVa: fusiform or cystic dilatation of intra- and extrahepatic ducts IVb: multiple cysts of extrahepatic ducts only | Congenital choledochal cysts | Todani types I and IV are combined as a spectrum of extrahepatic dilatation with varying intrahepatic involvement | 90% of cases: related to common channel syndrome. 10% of cases: primary biliary strictures, ganglion cell insufficiency, abnormal congenital recanalization, and reovirus infection |
| V | Intrahepatic dilatation only With fibrosis: Caroli syndrome | Caroli disease and syndrome | Congenital communicating intrahepatic duct dilatation With fibrosis: Caroli syndrome | Autosomal recessive disorder of ductal plate remodeling |

Sources.—References 5, 6.

disease (11). Patients often present with pain, jaundice, and/or recurrent cholangitis (9).

At imaging, Caroli disease appears as segmental cystic dilatation of the intrahepatic bile ducts. Liver involvement ranges from focal to diffuse. Demonstration of communication of the cystic malformation with intrahepatic ducts on conventional T2-weighted MRCP images or with hepatobiliary contrast material allows differentiation of Caroli disease from parenchymal and peribiliary cysts. Punctate enhancement formed by portal vein and hepatic artery branch vessels surrounded by the dilated intrahepatic duct constitutes the “central dot” sign and allows differentiation of Caroli disease from cysts (Fig 4) (9,11). The central dot sign can also help to

differentiate focal Caroli disease from other causes of focal biliary dilatation such as cholangiocarcinoma or an intra-ductal papillary mucinous neoplasm of the bile ducts (IPNB) (Fig 5). Complications arise due to bile stasis and include biliary stones, recurrent cholangitis, abscesses, cirrhosis, or cholangiocarcinoma (9,11). Treatment entails management of complications (eg, stone removal and cyst drainage), partial hepatectomy for focal Caroli disease, or liver transplant for diffuse disease throughout the liver (9).

Choledocholithiasis

Choledocholithiasis is the most common cause of biliary dilatation, usually secondary to passage of stones from

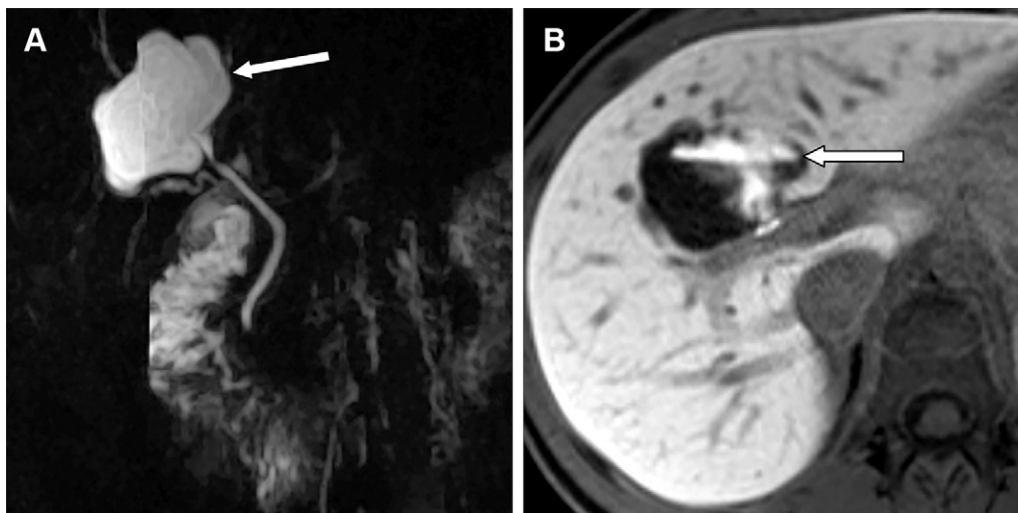


Figure 3. Use of hepatobiliary contrast material to evaluate a cystic hepatic lesion in an asymptomatic 14-year-old adolescent girl. **(A)** MRCP image shows a large hepatic cystic lesion (arrow), but communication between the cystic lesion and the biliary tree could not be definitively ascertained from conventional MRCP. **(B)** Axial gadobutate-enhanced hepatobiliary phase MR image shows excretion into the cystic lesion (arrow), confirming ductal communication with the extrahepatic duct, consistent with a Todani type II choledochal cyst.

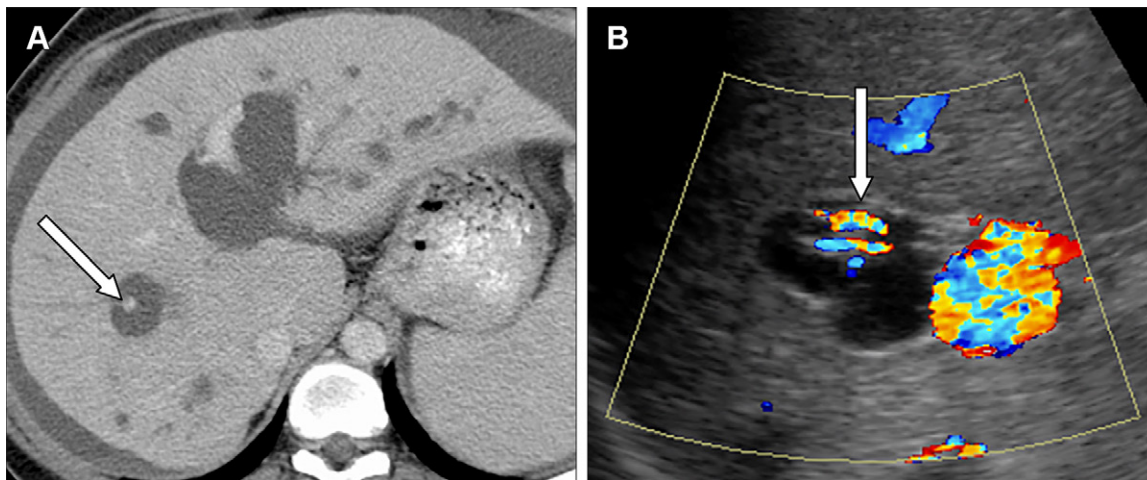


Figure 4. Caroli disease in a 22-year-old woman with a history of autosomal recessive polycystic kidney disease and congenital hepatic fibrosis. **(A)** Axial contrast-enhanced CT image shows multiple hypoattenuating lesions in the liver demonstrating the central dot sign (arrow). **(B)** Color Doppler US image shows that the central dot sign corresponds to flow in the branch vessels (arrow), which are surrounded by the dilated duct.

the gallbladder, which occurs in up to 16% of patients with cholelithiasis (12). Primary stone formation (typically pigment stones) occurs due to stasis or infection, but it is rare in the common duct (12,13). Biliary stones are often asymptomatic if they are smaller than 5 mm, but impaction or passage of larger stones can lead to cholangitis or pancreatitis.

US is the first-line modality for evaluating suspected stone disease, but visualization of distal common bile duct stones can be limited by bowel gas. Biliary stones typically appear as echogenic filling defects with posterior shadowing, although shadowing may be absent with stones smaller than 3 mm (14). Intraluminal debris, hemorrhage, or a neoplasm can mimic a nonshadowing stone, although these findings are usually less echogenic (13). On CT images, choledocholithiasis can appear as a central or dependent filling defect in the common duct, with surrounding low-attenuation bile. The attenuation of the stone varies based on composition (ie, cholesterol, calcification, or gas fissuring), with many isoattenuating to bile and thus occult on CT images (15). Biliary dilatation with abrupt duct cutoff may be the only clue to the presence of a CT-occult stone, an appearance similar to that of an obstructing neoplasm (16). Dual-energy CT can improve visualization of

stones on low-kiloelectron voltage monoenergetic and virtual noncontrast-enhanced CT images and differentiation of stones from an enhancing mass through comparison of virtual non-contrast-enhanced CT images to the iodine mapping CT images (Figs 6, S2) (17). On MR images, biliary stones are T2 hypointense and T1 variable, with cholesterol stones hypointense and pigmented stones hyperintense (18).

Mirizzi Syndrome

Mirizzi syndrome refers to extrahepatic duct obstruction from extrinsic compression, typically due to an impacted gallstone in the gallbladder neck or cystic duct, causing painless jaundice, cholangitis, or cholecystitis (Fig 7). A long cystic duct coursing parallel to the extrahepatic duct with low insertion predisposes patients to this condition. Accurate preoperative diagnosis helps to avoid the extrahepatic duct being mistaken for the cystic duct during surgery (19). Mirizzi syndrome should be considered when imaging shows biliary dilatation proximal to the mid extrahepatic duct without a common duct stone or mass. Identifying extrinsic compression of the extrahepatic duct by a gallbladder neck or cystic duct stone confirms the diagnosis.



Figure 5. Caroli disease in a 55-year-old woman with a focal dilated duct and suspected cholangiocarcinoma. Coronal (**A**) and axial (**B**) contrast-enhanced T1-weighted fat-suppressed MR images show a single focally dilated right intrahepatic duct (arrow). The patient underwent surgical resection due to suspicion for cholangiocarcinoma. Final pathologic results demonstrated focal Caroli disease, rather than cholangiocarcinoma. In retrospect, a subtle central dot sign is seen on **B**.



Figure 6. Choledocholithiasis in a 78-year-old woman with jaundice. (**A**) Coronal contrast-enhanced dual-energy CT image shows a suggestion of a round hyperattenuating filling defect in the distal common bile duct (arrow), with upstream biliary dilatation. (**B**) Axial contrast-enhanced CT image at the level of the distal common duct filling defect again shows a round hyperattenuating filling defect (arrow) with a surrounding crescent of low-attenuation bile. (**C**) Axial virtual noncontrast reformatted CT image nicely illustrates that the filling defect is hyperattenuating (arrow), favoring a calcified stone rather than an enhancing mass. A common bile duct stone was confirmed with endoscopic US and endoscopic retrograde cholangiopancreatography (ERCP).

Extrahepatic duct compression and obstruction may result from gallbladder cancer extending along the cystic duct, resulting in a similar imaging appearance sometimes referred to as malignant Mirizzi syndrome (20). Gallbladder cancer can also coexist with gallstone-related Mirizzi syndrome in up to 5.3% of cases due to biliary stasis and chronic inflammation and should be suspected when there is enhancing irregular wall thickening or an intraluminal mass (Fig 8) (21).

Neoplasms

Intraductal Papillary Neoplasm of the Bile Duct

IPNB is a rare biliary neoplasm and a precursor for cholangiocarcinoma. Clinical risk factors vary geographically: In Asia, major risk factors are *Clonorchis* infection and hepatolithiasis, whereas in Western countries, primary sclerosing cholangitis (PSC) and choledochal cysts are more common risk factors.

Similar to the analogous pancreatic intraductal papillary mucinous neoplasm, IPNB is characterized by intraductal papillary proliferation of epithelial cells lining a fibrovascular core and may show areas of solid or tubular growth (22). The fibrovascular core can be enlarged by edema or inflammatory cells. Mucin production is less common in IPNBs (33%) than it is in intraductal papillary mucinous neoplasms (100%) (23). Heterogeneity in cellular subtypes and associated differences in growth patterns and invasiveness have resulted in controversy regarding precise histologic criteria and molecular classification of IPNB (24,25). Type 1 IPNBs typically arise in intrahepatic ducts, commonly show mucin production, often include both low- and high-grade dysplasia, and demonstrate invasive components in approximately 50% of cases (25). Type 2 IPNBs (also called papillary carcinoma or cholangiocarcinoma type IPNB) typically arise in extrahepatic ducts, infrequently produce substantial mucin, and always show high-grade dysplasia, with an invasive component present in

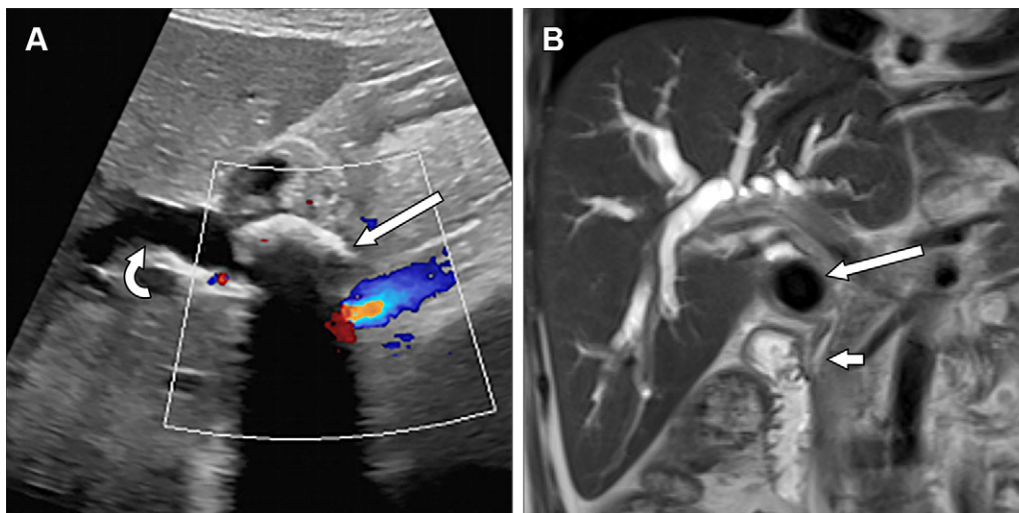


Figure 7. Mirizzi syndrome in a 59-year-old woman who presented with jaundice, pruritis, and an elevated bilirubin level. **(A)** Transverse color Doppler US image shows a large shadowing stone in the gallbladder neck (straight arrow), with upstream ductal dilatation (curved arrow). Note the partially visualized gallbladder wall, which is thickened and irregular. **(B)** Coronal T2-weighted MR image shows a large ovoid hypointense stone (long arrow) narrowing the extrahepatic duct at the expected level of the cystic duct insertion. The upstream intrahepatic and extrahepatic ducts are markedly dilated, with the distal common bile duct normal in caliber (short arrow). Findings at surgery and pathologic evaluation confirmed Mirizzi syndrome due to a large gallstone and acute and chronic cholecystitis.

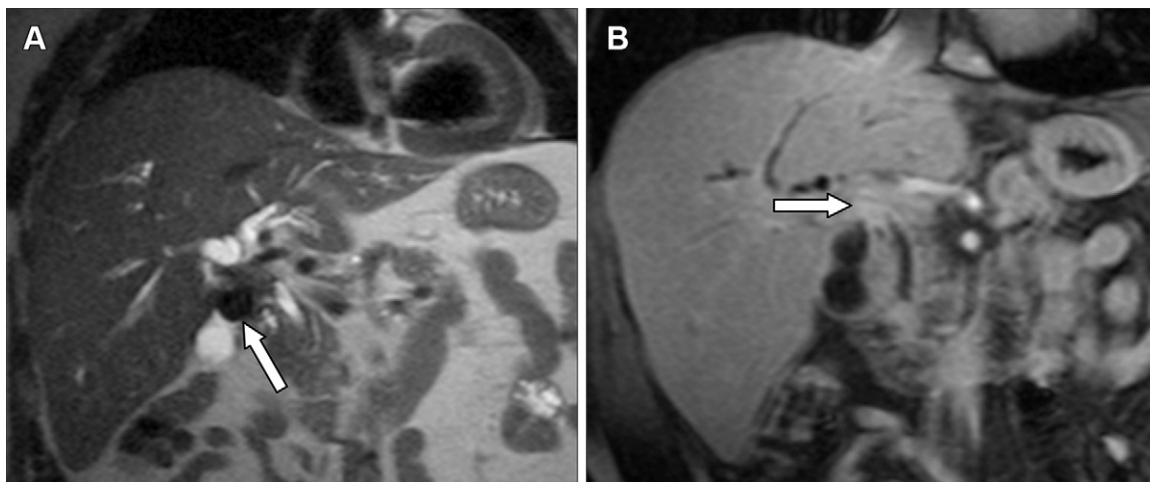


Figure 8. Malignant Mirizzi syndrome, with gallbladder carcinoma manifesting as a malignant stricture at the cystic duct insertion in a 58-year-old man. **(A)** Coronal T2-weighted MR image shows a hypointense stone in the gallbladder neck narrowing the common hepatic duct and causing upstream biliary dilatation (arrow), indicative of Mirizzi syndrome. **(B)** Coronal contrast-enhanced T1-weighted fat-suppressed MR image shows thickening and enhancement of the gallbladder neck wall adjacent to the stone (arrow), suggesting the presence of a soft-tissue neoplasm in addition to the gallbladder neck stone. Pathologic evaluation at cholecystectomy revealed gallbladder adenocarcinoma.

greater than 90% of cases (25). Thus, there are controversies about whether these IPNB types represent a single entity and whether they are distinct from, overlap with, or exist entirely on the same spectrum as conventional cholangiocarcinomas. Nevertheless, the majority of clinically detectable IPNBs have a malignant component, although extraductal invasion is only identifiable at imaging in 28% of cases (Figs 9, S3) (26,27). The prognosis for IPNB with invasive cholangiocarcinoma is better than that for other cholangiocarcinomas (27).

At US, an intraductal filling defect representing a mass can be seen in up to 41% of cases (28). The mucinous com-

ponent is anechoic, similar to bile, and thus undetectable. Contrast-enhanced US may help to distinguish a solid mass from sludge or stones (29). At MRI, biliary dilatation is often seen, either due to solid intraluminal papillary lesions or the thick, viscous mucin itself (28). The solid component of IPNB appears hypointense on T1-weighted MR images and shows intermediate signal intensity on T2-weighted MR images, with variable enhancement more appreciable at MRI than at CT (Fig 10) (26). Diffusion restriction may be seen in the solid component and helps to show tumor invasion into the hepatic parenchyma. The mucinous component may be

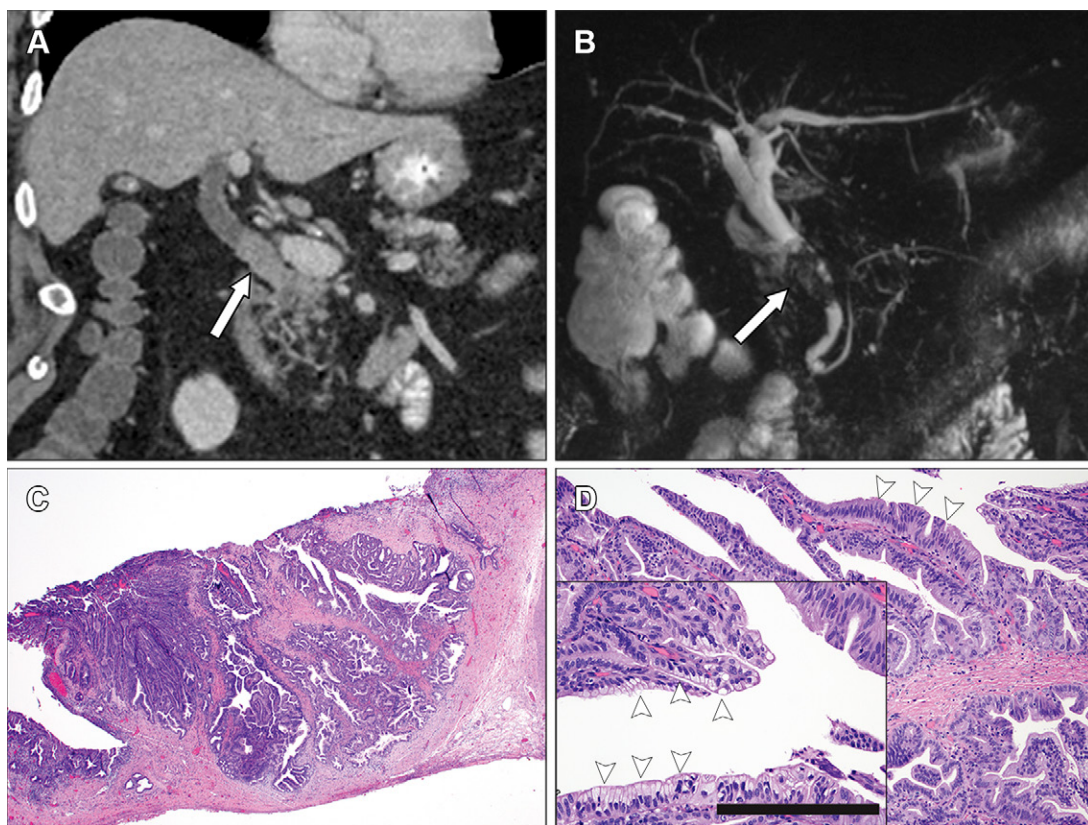


Figure 9. Invasive carcinoma arising in an IPNB in a 75-year-old man undergoing evaluation for anorexia. **(A)** Coronal contrast-enhanced CT image obtained for initial workup shows a soft-tissue polypoid lesion in and expanding the distal common bile duct (arrow). **(B)** Coronal MIP MRCP image shows the mass as a polypoid filling defect in the common duct (arrow), resulting in upstream biliary dilatation. Similar findings were seen at ERCP, and the mass was also visualized at endoscopic US (Fig S3). Based on the imaging appearance, it is difficult to distinguish noninvasive IPNB from intraductal cholangiocarcinoma arising in an IPNB. The patient subsequently underwent the Whipple procedure for resection of the common duct mass. Pathologic examination of the resection specimen showed an intraductal papillary neoplasm of the bile duct with a subcentimeter focus of invasive cholangiocarcinoma. **(C)** Photomicrograph shows the common bile duct lumen occupied by neoplastic proliferation of biliary epithelium forming arborizing papillary structures. (Hematoxylin-eosin stain; original magnification, $\times 20$; scale bar = $500\mu\text{m}$.) **(D)** Photomicrograph shows elongated papillary structures with slender fibrovascular cores (arrowheads), and inset photomicrograph shows intracytoplasmic mucin (arrowheads) in the neoplastic epithelial lining. (Hematoxylin-eosin stain; original magnification, $\times 200$ [inset, $\times 400$]; scale bar = $200\mu\text{m}$.)

indistinguishable from bile or may demonstrate stringlike filling defects on MRCP images (ie, the “thread sign”). A combination of intraluminal papillary filling defects with arterial enhancement and early washout plus associated upstream and downstream biliary ductal dilatation is highly suggestive of IPNB. However, variability in the extent of the solid component and mucin production results in a spectrum of imaging appearances, from a solid biliary mass with upstream biliary dilatation, to focal (sometimes cystic) duct dilatation from mucin production without a visible mass (25,30). Imaging mimics of IPNB include obstructing lesions such as hepatolithiasis and cholangiocarcinoma, causes of focal biliary dilatation such as choledochal cysts, and hepatic mucinous cystic neoplasms. Endoscopic evaluation can be particularly helpful when a discrete mass is not seen at MRI or MRCP, either because of detection of mucin on endoscopic retrograde cholangiopancreatography (ERCP) or direct visualization of an associated mass using cholangioscopy (31).

Cholangiocarcinoma

Definition, Pathogenesis, and Classification.—Cholangiocarcinoma refers to adenocarcinoma of the bile ducts and accounts for 3% of gastrointestinal malignancies in the United States (32–34). Cholangiocarcinoma arises from the epithelial lining of bile ducts, peribiliary glands, or progenitor cells and hepatocytes (35), usually in patients with chronic inflammation and bile stasis (36). Based on current classification (32), adenocarcinomas arising from the gallbladder and ampulla of Vater are considered separate entities from cholangiocarcinoma.

Anatomically, cholangiocarcinomas are divided into intrahepatic, perihilar (most common), and distal types (32). Intrahepatic cholangiocarcinomas have recently been divided into small duct (composed of nonmucin-producing cuboidal cells) and large duct types (composed of mucin-producing cells). PSC, hepatobiliary parasites, and

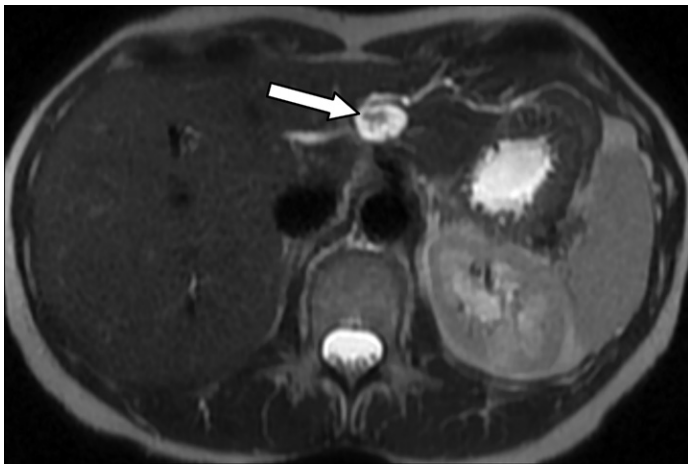


Figure 10. Intraductal papillary neoplasm of the bile duct in a 63-year-old woman. Axial T2-weighted MR image shows dilatation of the left intrahepatic ducts, with a focal cystic lesion in continuity with the ducts. The cystic morphology of dilatation is more commonly seen in intrahepatic IPNB than in extrahepatic IPNB, which typically demonstrates fusiform ductal dilatation. A papillary hypointense component projects into the cystic lesion (arrow). Pathologic evaluation showed an intraductal papillary neoplasm of the bile duct with dysplasia but no invasive carcinoma. (Case courtesy of Paul Nolan, MD, Advocate Health Care, Chicago, Ill.)

hepatolithiasis are major risk factors for large duct cholangiocarcinoma. Biliary intraepithelial neoplasia and IPNB are precursor lesions of large duct intrahepatic cholangiocarcinomas (as well as perihilar and distal cholangiocarcinoma) but not small duct intrahepatic cholangiocarcinomas (33,36) and share common molecular alterations including *KRAS* and *TP53* mutations (37,38). Small duct intrahepatic cholangiocarcinomas have similar risk factors to those of hepatocellular carcinoma and a more favorable prognosis than large duct intrahepatic cholangiocarcinomas (33,36).

Cholangiocarcinomas demonstrate three main growth patterns: mass-forming, periductal infiltrating, and intraductal patterns or a combination thereof. Mass-forming growth is the most common pattern in small duct intrahepatic cholangiocarcinomas, manifesting as a fibrous mass with necrotic areas. The periductal infiltrating pattern, the most common pattern for large duct intrahepatic cholangiocarcinomas and perihilar and distal cholangiocarcinomas, manifests as strictures and ductal wall thickening. Most intraductal types are now considered malignant transformations of IPNB and are common in perihilar and distal cholangiocarcinoma (33).

Because brushing and endoscopic US-guided fine-needle aspiration usually yield scant tissue, histopathologic results may not be conclusive or definitive. Next-generation sequencing is performed at some institutions to increase sensitivity for detection of cholangiocarcinoma (39). Due to an overlap in histologic findings, differentiation among pancreatic adenocarcinoma, gallbladder carcinoma, metastasis, and cholangiocarcinoma can be challenging based on histopathologic examination alone, emphasizing the importance of imaging.

Imaging Findings and the Role of Imaging for Assessment of Resectability.—Imaging findings of intrahepatic cholangiocarcinoma mirror their histopathologic features. Intrahepatic cholangiocarcinoma manifesting as a discrete parenchymal mass shows variable degrees of fibrosis, necrosis, and heterogeneity (40). They usually have lower T1 and variable T2 signal intensity compared with the background liver and early peripheral enhancement, with progressive or delayed enhancement due to their characteristic fibrous stroma. Central T2 hypointensity reflecting central fibrosis can be seen. The fibrous stroma accounts for capsular retraction seen with peripheral lesions and upstream biliary dilatation (40). Despite the typical findings of intrahepatic cholangiocarcinomas, imaging features can mimic hepatocellular carcinoma and combined hepatocellular carcinoma-cholangiocarcinoma with arterial enhancement and delayed washout, and definitive diagnosis requires tissue sampling. Because large duct intrahepatic cholangiocarcinomas can arise from IPNB, they may appear similarly as polypoid intraductal masses (Fig 11).

Imaging evaluation of perihilar and distal cholangiocarcinomas is more challenging given the overlapping appearance with other benign and malignant processes. Biliary stricture and upstream dilatation are the hallmarks of these cholangiocarcinoma types (Fig 12). Depending on the stage, an associated periductal mass may be seen. MRI or MRCP is advantageous for staging, although some institutions prefer CT. Patients typically undergo ERCP for tissue sampling for confirmation of the diagnosis and stenting for relief of obstruction. MRI and MRCP should be performed before ERCP to avoid postprocedural ductal inflammation confounding the staging. Special attention should be given to hilar vascular involvement because this affects tumor resectability. Severe narrowing or occlusion of a major portal vein branch often leads to atrophy of the supplied liver lobe and compensatory hypertrophy of the unaffected lobe, resulting in the “atrophy-hypertrophy” sign, which is more pronounced when the ipsilateral bile duct is also occluded. PET/CT is most useful for evaluation of nodal and distant metastases (41).

Surgical and Clinical Staging and Classification.—Surgical resection with negative margins provides the best chance for long-term survival (42). A liver transplant is another curative method offered to selected patients. Intrahepatic cholangiocarcinoma and distal cholangiocarcinoma tend to be more amenable for surgical resection through hepatic resection and pancreaticoduodenectomy, respectively. Resection with negative margins is difficult to achieve for perihilar cholangiocarcinomas due to frequent bilobar and vascular involvement. Various classification systems have been used to help determine surgical resectability of perihilar cholangiocarcinomas, including the Bismuth-Corlette (Fig 13) and the Memorial Sloan-Kettering Cancer Center classification systems (43,44).

Preoperative imaging and reporting must provide thorough evaluation of hepatic vessels, bile ducts, regional and distant lymph nodes, and distant metastases to optimize patient selection for surgical resection. Assessment of resectability varies by institution and may be best addressed by multidisciplinary review. With new surgical techniques,

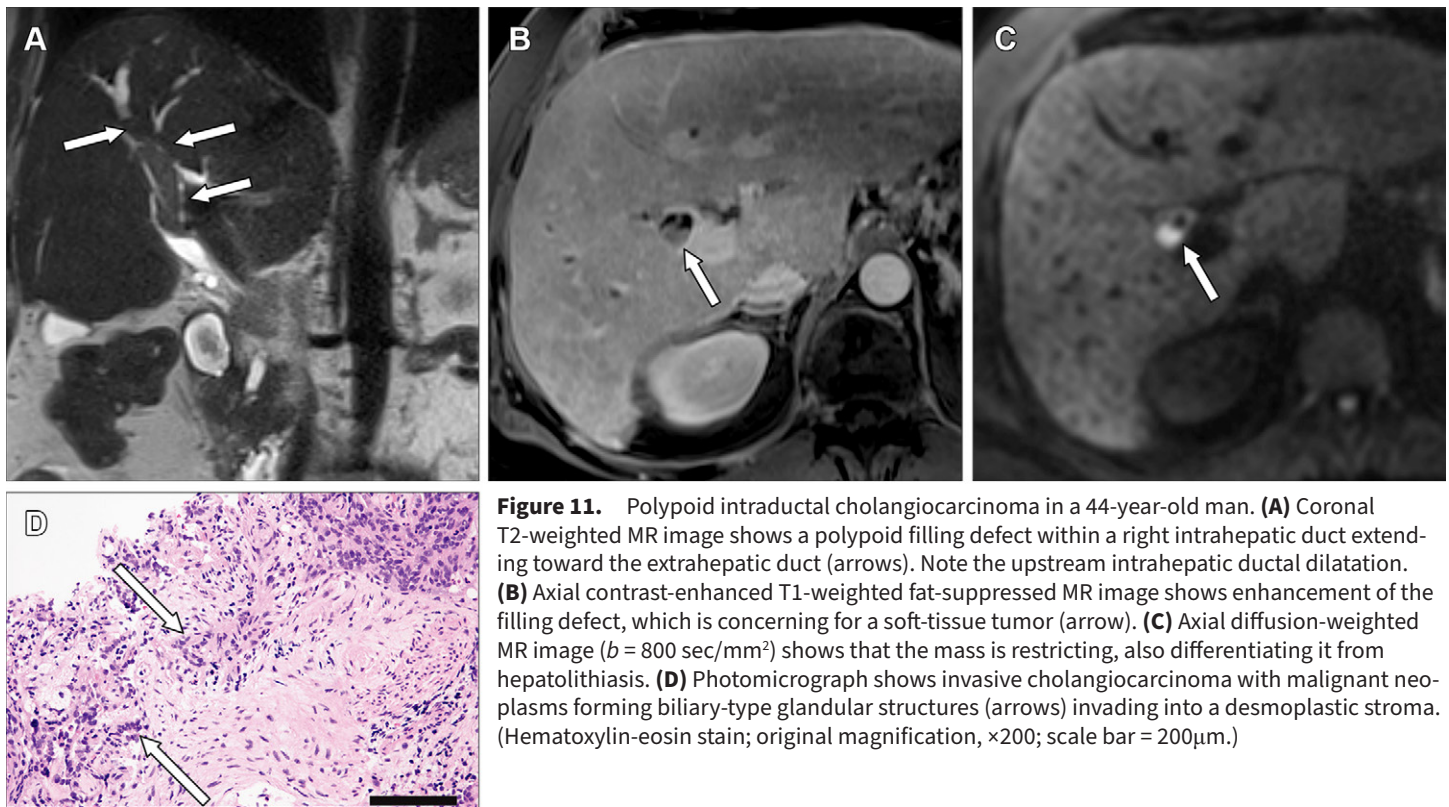


Figure 11. Polypoid intraductal cholangiocarcinoma in a 44-year-old man. **(A)** Coronal T2-weighted MR image shows a polypoid filling defect within a right intrahepatic duct extending toward the extrahepatic duct (arrows). Note the upstream intrahepatic ductal dilatation. **(B)** Axial contrast-enhanced T1-weighted fat-suppressed MR image shows enhancement of the filling defect, which is concerning for a soft-tissue tumor (arrow). **(C)** Axial diffusion-weighted MR image ($b = 800 \text{ sec/mm}^2$) shows that the mass is restricting, also differentiating it from hepatolithiasis. **(D)** Photomicrograph shows invasive cholangiocarcinoma with malignant neoplasms forming biliary-type glandular structures (arrows) invading into a desmoplastic stroma. (Hematoxylin-eosin stain; original magnification, $\times 200$; scale bar = $200\mu\text{m}$.)

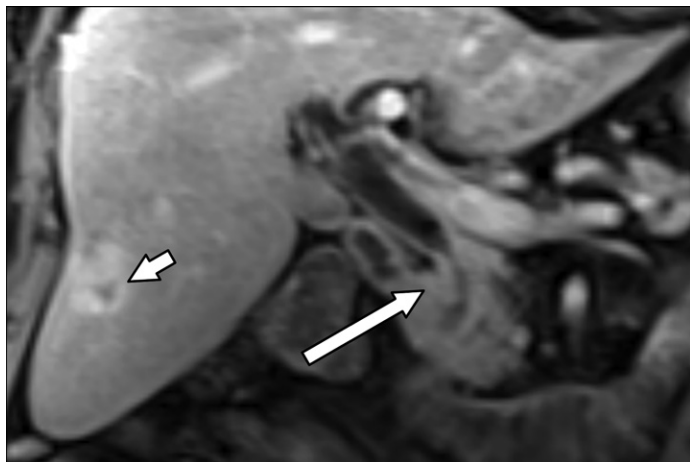


Figure 12. Periductal infiltrating cholangiocarcinoma causing distal common bile duct stricture in a 66-year-old man. Coronal contrast-enhanced T1-weighted fat-suppressed MR image depicts a long stricture of the distal common bile duct with asymmetric wall thickening and a shouldered appearance at the margins (long arrow), compatible with malignant stricture. Note the rim-enhancing liver metastasis (short arrow).

contralateral vascular involvement is no longer a definite contraindication for resection, so the extent of vascular involvement should be described in these situations (45). Evaluation of vascular involvement is similar to evaluation of pancreatic cancer, with a determination of no contact, abutment (<50% of vessel circumference involved), or encasement (>50% of vessel circumference involved) (46). A structured reporting template can help to ensure that important structures are

assessed (Table 3) (46). Given the importance of accurate assessment of vascular involvement in determining resectability, CT angiography, with its high spatial resolution, may be warranted in challenging cases.

Metastases and Other Neoplasms

Liver metastases, lymphoma, or gallbladder cancer can compress or obstruct the bile ducts. Metastases to the bile ducts themselves are rare but may be seen with adenocarcinomas (eg, of the colon, pancreas, stomach, breast, or endometrium), (Fig S4), melanoma, and lymphoma (47). Biliary obstruction or occlusion from liver or biliary metastases should be described to help determine the necessity of and guide procedures for decompression of the dilated ducts.

Cholangitis and Ischemic Disease

Acute Bacterial Cholangitis

Acute bacterial (“ascending”) cholangitis is caused by a gram-negative bacterial infection, frequently seen in patients with choledocholithiasis but possible with any cause of biliary obstruction. Mechanisms include retrograde contamination from the gastrointestinal tract (often facilitated by stents or scopes traversing the ampulla), seeding from the portal vein, or percutaneous biliary procedures (48). Obstruction is crucial to the pathogenesis of acute bacterial cholangitis, with higher biliary pressure levels promoting entrance of bacteria into the bloodstream and resulting in more severe illness. Symptoms include fever, pain, and jaundice (ie, the Charcot triad) and may progress to lethargy and shock (ie, Reynolds pentad).

Imaging can show biliary inflammation and allow identification of the associated obstruction and complications. US

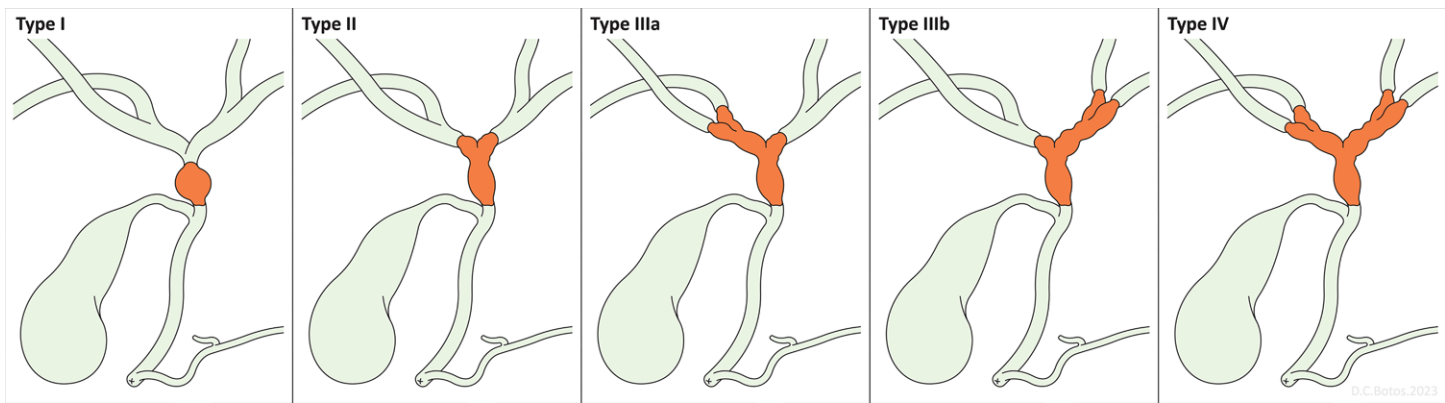


Figure 13. Illustrations show the Bismuth-Corlette classification system for perihilar cholangiocarcinoma. Type I = tumor is distal to the right and left hepatic duct confluence. Type II = tumor involves the hepatic duct confluence. Type III = tumor involves the hepatic duct confluence and the proximal right (type IIIa) or left (type IIIb) hepatic duct. Type IV = tumor involves the hepatic duct confluence and bilateral proximal hepatic ducts.

can show ductal dilatation, but CT or MRI may allow better identification of the cause of obstruction. Intrahepatic ductal dilatation is usually present, with extrahepatic dilatation depending on the level of obstruction (49). Bile duct wall thickening and hyperenhancement are characteristic features. Periductal edema may be present, appearing as periductal hypoattenuation on CT images and T2 hyperintensity on MR images (50). Heterogeneous hepatic hyperenhancement during arterial phase imaging (Fig 14) can result from compensatory arterial flow in areas of inflammation-related venous congestion and/or biliary stasis. Repeated cholangitis episodes result in ductal irregularity that may resemble PSC or recurrent pyogenic cholangitis, although the clinical context usually allows differentiation of these entities.

Recurrent Pyogenic Cholangitis

Recurrent pyogenic cholangitis is the result of chronic biliary inflammation due to recurrent infection leading to strictures, dilatation, and hepatolithiasis. The cause is unclear, but it is postulated that colonization of the biliary tree by *Clonorchis* or *Ascaris* parasites leads to strictures, stasis, and recurrent bacterial superinfection (51). The disease is more prevalent in East and Southeast Asia, although the incidence in the United States is increasing with emigration from endemic areas.

Recurrent pyogenic cholangitis should be suspected when intrahepatic pigmented stones (present in 90% of cases) (51,52) and biliary dilatation accompany recurrent cholangitis. The central intrahepatic ducts are typically disproportionately dilated, with abrupt peripheral tapering (ie, the “arrowhead” sign) and/or short strictures (Fig 15, S5). The extrahepatic duct is often diffusely dilated but rarely demonstrates strictures (51). On MRCP images, stones appear as filling defects in the ducts, forming the “missing duct” sign (52). Intrahepatic and common bile duct stones (usually T1-hyperintense pigment stones at MRCP) without gallstones should prompt evaluation for causes of chronic biliary stasis including recurrent pyogenic cholangitis, PSC, or Caroli disease. Prominent central intrahepatic duct dilatation favors recurrent pyogenic cholangitis, while a beaded appearance favors PSC.

Episodes of acute inflammation may demonstrate ductal wall thickening and hyperenhancement, in addition to the typical findings of altered ductal morphology and hepatolithiasis. Abscesses are seen in up to 20% of patients and can be differentiated from bilomas by their thicker rim enhancement (52) and restricted diffusion on MR images. Hepatic atrophy and cirrhosis may develop, most frequently in the lateral left lobe and posterior right lobe. Cholangiocarcinoma occurs in up to 5% of patients, typically in atrophic or heavily stone-burdened segments. The risk of hepatocellular carcinoma is also elevated, particularly if cirrhosis has developed (52).

Primary Sclerosing Cholangitis

PSC is an idiopathic cholestatic disease characterized by inflammation and fibrosis of the bile ducts resulting in multifocal strictures (53). PSC is strongly associated with inflammatory bowel disease, predominantly ulcerative colitis.

MRI or MRCP has replaced ERCP for diagnosis and surveillance imaging. Intrahepatic biliary strictures are the hallmark of PSC. Extrahepatic ducts may also be involved, but isolated extrahepatic abnormality is rare. Multifocal strictures alternating with segments of normal-caliber or mildly dilated ducts cause the classic beaded appearance of the ducts. Periductal fibrosis restricts ductal dilatation; thus, bile ducts are usually not markedly dilated in uncomplicated PSC, even upstream from strictures (54). In advanced disease, obliteration of peripheral intrahepatic ducts results in the “pruned tree” appearance of PSC. Active inflammation can appear as bile duct wall thickening and enhancement, which are often associated with heterogeneity of the peripheral liver parenchyma (Fig 16). Chronic PSC may result in portal hypertension and cirrhosis, with characteristic morphologic changes including caudate hypertrophy with left lateral and right posterior segment atrophy resulting in a rounded liver appearance (54).

PSC is associated with multiple malignancies including cholangiocarcinoma, gallbladder carcinoma, and hepatocellular carcinoma. Among these, cholangiocarcinoma is the most common, with an estimated annual incidence of 0.5%–1.5% (55,56) and a lifetime incidence of 10% (57). Patients with PSC develop cholangiocarcinoma at a younger age than

Table 3: Perihilar Cholangiocarcinoma Reporting Template

| |
|---|
| Tumor size (including the radial size) |
| Intrahepatic satellite lesions: No/Yes (specify location) |
| Involved bile ducts: |
| <input type="checkbox"/> Biliary confluence |
| <input type="checkbox"/> Common hepatic duct |
| <input type="checkbox"/> Common bile duct |
| <input type="checkbox"/> Right hepatic duct |
| <input type="checkbox"/> Left hepatic duct |
| <input type="checkbox"/> Cystic duct |
| <input type="checkbox"/> Right secondary confluence |
| <input type="checkbox"/> Left secondary confluence |
| <input type="checkbox"/> Caudate duct |
| Variant biliary anatomy: No/Yes (specify)/Not evaluable |
| Variant arterial anatomy: No/Yes (specify)/Not evaluable |
| Arterial involvement: |
| <input type="checkbox"/> Proper hepatic artery (intact/stranding/soft-tissue abutment/soft-tissue encasement) |
| <input type="checkbox"/> Right hepatic artery (intact/stranding/soft-tissue abutment/soft-tissue encasement) |
| <input type="checkbox"/> Left hepatic artery (intact/stranding/soft-tissue abutment/soft-tissue encasement) |
| <input type="checkbox"/> Common hepatic, celiac, superior mesenteric, others (intact/stranding/soft-tissue abutment/soft-tissue encasement) |
| Variant portal venous anatomy: No/Yes (specify)/Not evaluable |
| Portal venous involvement: |
| <input type="checkbox"/> Main portal vein (intact/stranding/soft-tissue abutment/soft-tissue encasement) |
| <input type="checkbox"/> Right portal vein (intact/stranding/soft-tissue abutment/soft-tissue encasement) |
| <input type="checkbox"/> Left portal vein (intact/stranding/soft-tissue abutment/soft-tissue encasement) |
| Lobar atrophy or hypertrophy: No/Yes (specify) |
| Future liver remnant volume (if applicable) |
| Nodal status: |
| <input type="checkbox"/> Suspicious regional lymph nodes: No/Yes (periportal, portocaval, hepatic artery) |
| <input type="checkbox"/> Suspicious distant lymph nodes: No/Yes |
| Distant metastasis: No/Yes |
| Peritoneal carcinomatosis: No/Yes |
| Source.—Reference 46. |

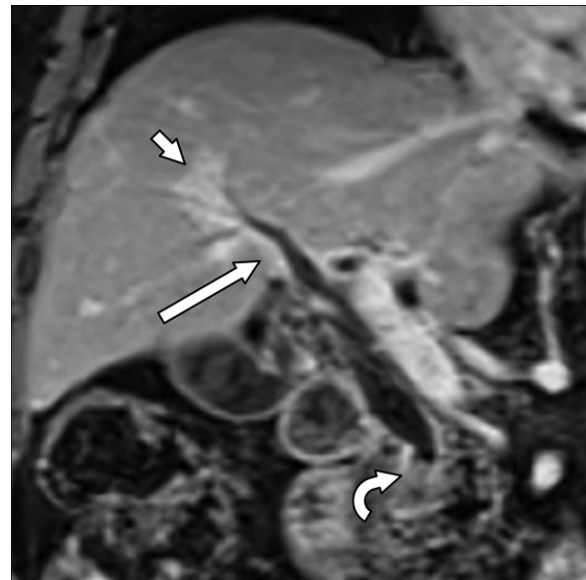


Figure 14. Acute cholangitis due to choledocholithiasis in a 76-year-old man with gallstones. Coronal contrast-enhanced T1-weighted MR image shows a stone in the distal common bile duct (curved arrow) causing upstream ductal dilation. Thickening and hyperenhancement of the bile duct wall are present (long straight arrow) with patchy periductal liver parenchymal hyperenhancement (short straight arrow).

cinoma (Fig 17). Identification of a high-grade stricture is also suspicious and warrants ERCP, particularly if it is associated with periductal thickening or worsening lobar atrophy (53). ERCP literature describes specific duct luminal diameters required for diagnosing a dominant stricture, and MRCP may not precisely correlate due to a lack of active biliary distention. In addition, a standard definition and management strategy for dominant strictures is not universally agreed on among members of various medical specialties. Therefore, some advocate for using terminology of *low-grade* (<75% luminal narrowing) and *high-grade* (>75%) rather than *dominant* stricture when reporting MRCP findings (53). The gallbladder should also be assessed for eccentric wall thickening, polyps, or masses. The lifetime risk of gallbladder carcinoma in patients with PSC is greater than that in the general population (reported as 3%–14%), and close follow-up or cholecystectomy should be considered for polyps in these patients (58).

Immunoglobulin G4-related Sclerosing Cholangitis

Immunoglobulin G4 (IgG4)-related sclerosing cholangitis is a benign autoimmune cholangitis characterized by transmural lymphoplasmacytic infiltrate in the biliary walls and peribiliary tissue with associated fibrosis. IgG4-sclerosing cholangitis mainly affects men in their 6th and 7th decades of life (59). It can manifest with jaundice and abdominal pain but is often asymptomatic and discovered with IgG4-related autoimmune pancreatitis, which is present in up to 90% of patients with IgG4 sclerosing cholangitis (60). An elevated serum IgG4 level (≥ 135 mg/dL) is characteristic, and the cholangitis responds well to corticosteroid therapy.

the general population do (ie, during the 4th decade of life or earlier), with one-half of patients diagnosed with cholangiocarcinoma concurrently or within 1 year of diagnosis of PSC (57). Given the high prevalence and mortality of cholangiocarcinoma in PSC, routine surveillance of patients with PSC with US, MRI, or MRCP in addition to serum cancer antigen (CA) 19-9 testing every 6–12 months is essential for early detection, with MRI more sensitive and specific than US (54). A progressively enhancing perihilar mass, an intraductal luminal mass, or focal periductal soft-tissue thickening with delayed enhancement or vascular narrowing encountered in a patient with PSC is highly suggestive of cholangiocar-

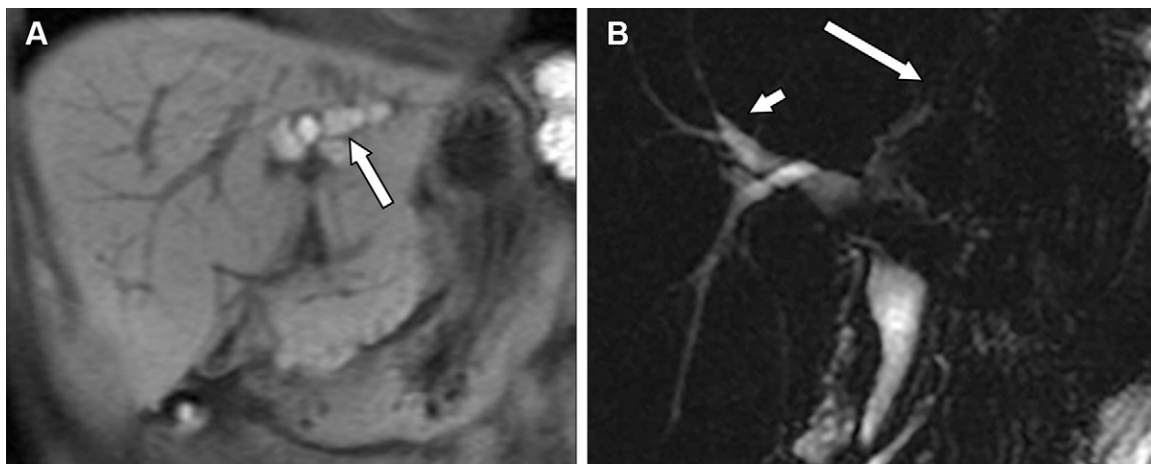


Figure 15. Recurrent pyogenic cholangitis in a 50-year-old woman with reports of prior abnormal imaging performed while she was out of the country. **(A)** Coronal unenhanced T1-weighted fat-suppressed MR image shows multiple intraductal hyperintense stones within a left hepatic lobe bile duct (arrow). **(B)** Coronal MIP MRCP image shows abrupt tapering of the right intrahepatic ducts constituting the “arrowhead sign” (short arrow). Nonvisualization of the left ducts due to intraductal stones constitutes the “missing duct” sign (long arrow). The extrahepatic duct is diffusely dilated, also characteristic of recurrent pyogenic cholangitis.

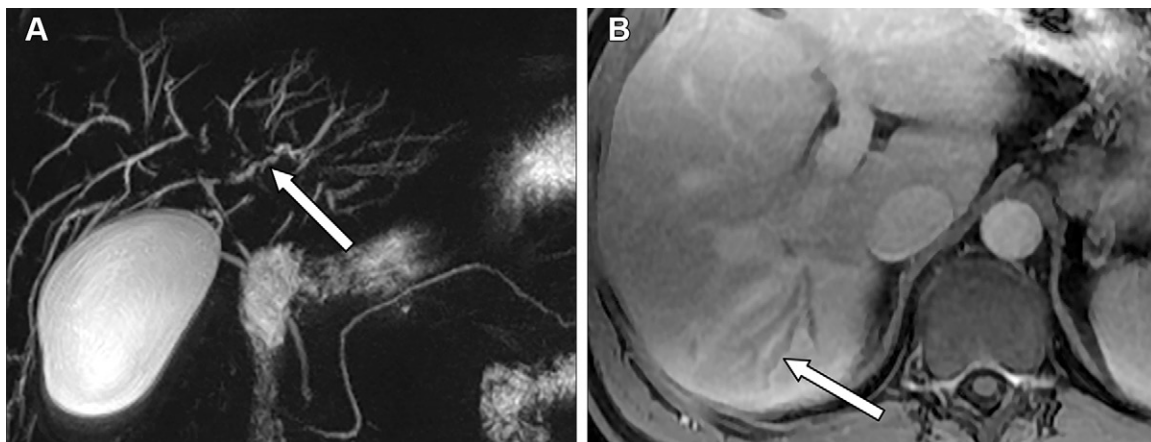


Figure 16. Primary sclerosing cholangitis in a 37-year-old man with Crohn disease. **(A)** Coronal MIP MRCP image shows irregularity of the intrahepatic ducts with alternating foci of narrowing and mild dilatation (arrow). **(B)** Axial contrast-enhanced T1-weighted MR image shows dilated intrahepatic ducts with ductal wall thickening, hyperenhancement (arrow), and surrounding parenchymal hyperenhancement compatible with active inflammation.

On biliary images, IgG4 sclerosing cholangitis may mimic other forms of cholangitis, especially PSC, but characteristic multiorgan involvement including pancreatic, renal, and salivary gland involvement and retroperitoneal fibrosis provide a diagnostic clue (Figs 18, S6). IgG4 sclerosing cholangitis can involve any level of the biliary tree, but the intrapancreatic portion of the common duct is usually affected (61). Strictures demonstrate circumferential smooth wall thickening, with homogeneous delayed enhancement, and tend to be longer than those seen in PSC. Unlike cholangiocarcinoma, which tends to cause asymmetric wall thickening and luminal obliteration, preservation of the lumen in the thickened segments is common with IgG4-sclerosing cholangitis.

COVID-19 Secondary Sclerosing Cholangitis

COVID-19 secondary sclerosing cholangitis is part of a wide range of extrapulmonary manifestations that can occur in

patients with a SARS-CoV-2 infection. Liver injury occurs in up to 45% of patients with COVID-19 and is associated with severe illness (62,63). Direct virus-induced cell damage, a cytokine storm, and drug-induced hepatotoxicity can all contribute to liver dysfunction. Expression of angiotensin-converting enzyme 2 receptor (the target for the virus’s spike protein) is 20 times greater on bile duct epithelial cells than on hepatocytes, suggesting that the biliary epithelium may be particularly susceptible to viral-induced injury. However, transaminitis is more common than γ -glutamyl transpeptidase and alkaline phosphatase elevation in COVID-19-associated liver injury (63), and further investigation may clarify the mechanisms of injury. Nevertheless, a subset of critically ill patients with COVID-19 develops rapidly progressive cholestatic liver injury, with features of sclerosing cholangitis. Diagnosis is based on a combination of clinical, laboratory, and imaging findings, with liver biopsy reserved

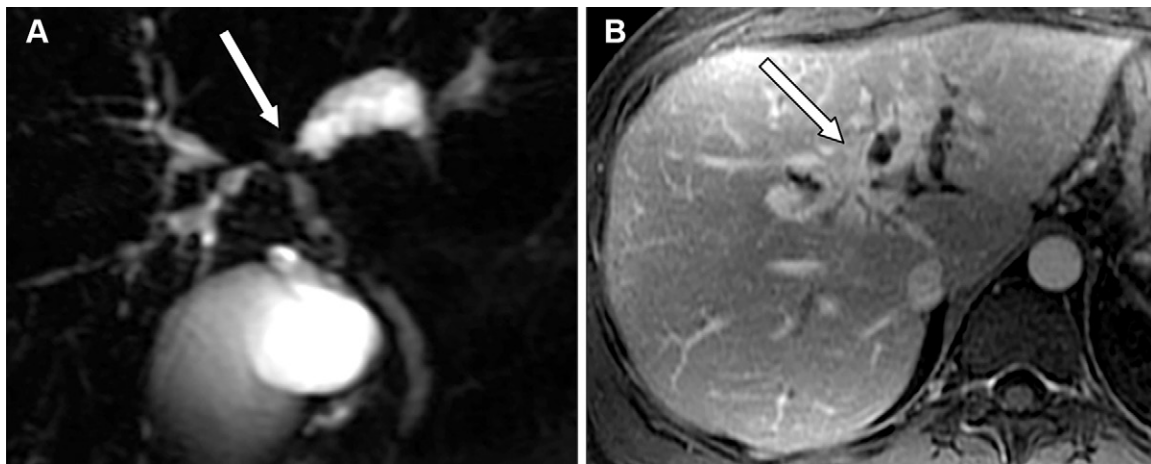


Figure 17. Cholangiocarcinoma in a 36-year-old man with primary sclerosing cholangitis. **(A)** Coronal MIP MRCP image shows a stricture at the confluence of the left and right hepatic ducts (arrow), with marked dilatation of the left intrahepatic ducts. Alternating foci of narrowing and dilatation in the right hepatic ducts and a paucity of peripheral ducts are compatible with a background of PSC. **(B)** Axial delayed phase contrast-enhanced T1-weighted fat-suppressed MR image shows biliary wall thickening and ill-defined masslike enhancement at the stricture (arrow). Brush biopsy results showed cholangiocarcinoma involving the left intrahepatic, right intrahepatic, and extrahepatic ducts.



Figure 18. IgG4-related sclerosing cholangitis in a 67-year-old man with a history of autoimmune pancreatitis and retroperitoneal fibrosis. **(A)** Coronal MIP MRCP image shows foci of narrowing and dilatation throughout the intrahepatic ducts. The appearance is reminiscent of PSC, although multiple small peripheral intrahepatic ductal branches are visualized, as opposed to the typical pruned appearance in PSC. Extrahepatic narrowing is most pronounced at the distal, intrapancreatic portion of the common bile duct (arrow), a characteristic location for involvement of IgG4-related sclerosing cholangitis. **(B)** Coronal contrast-enhanced T1-weighted fat-suppressed MR image shows the long extrahepatic duct stricture, with smooth wall thickening (arrow). Findings are typical of IgG4-related stricture. **(C)** Axial contrast-enhanced T1-weighted fat-suppressed MR image shows diffuse pancreatic enlargement with a hypointense peripheral rind (arrow). The multiorgan involvement with IgG4-related disease including autoimmune pancreatitis and retroperitoneal fibrosis (Fig S6) help to confirm the diagnosis of IgG4-related sclerosing cholangitis.

for inconclusive cases. A liver transplant may be needed in a significant minority of patients (62).

In a small cohort of patients with COVID-19 secondary sclerosing cholangitis, MRCP showed multifocal (usually bilobar) intrahepatic biliary strictures that were sometimes accompanied by biliary dilatation. Almost one-half of patients showed a “pruned tree” appearance of the biliary tree due to damaged peripheral ducts. The extrahepatic duct was usually not involved. Peribiliary edema and parenchymal signal intensity changes including patchy T2-weighted and diffusion-weighted MRI hyperintensity and arterial phase hyperenhancement were common (Fig 19). Although COVID-19 is known to cause vascular complications, hepatic macrovascular abnormalities were not seen in these patients, although imaging-occult microvascular insults may contribute to an ischemic component of biliary injury. Periportal lymphadenopathy was also not

seen in COVID-19 secondary sclerosing cholangitis, which is a potentially differentiating feature from PSC (62). However, given the substantial overlap in imaging appearance with PSC and other causes of cholangitis, the clinical context is essential for diagnosis.

Portal Cholangiopathy

Portal cholangiopathy (ie, portal biliopathy) is characterized by biliary morphologic changes and potential obstruction in patients with extrahepatic portal vein occlusion of any cause and subsequent formation of extensive peribiliary collateral veins in the porta hepatis (64). Portal cholangiopathy can be classified on the basis of pathogenesis and the presence of strictures into varicoid, fibrotic, or mixed types (65,66). The varicoid form manifests as extrinsic compression by enlarged collateral vessels causing smooth indentation of the extrahepatic bile duct

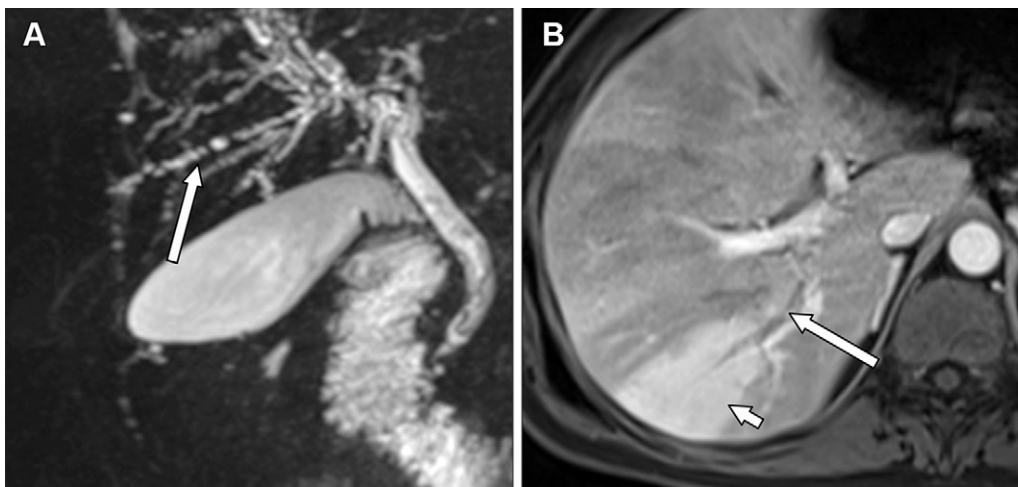


Figure 19. COVID-19 secondary sclerosing cholangitis in a 33-year-old man who recently underwent a bilateral lung transplant for COVID pneumonia and acute respiratory distress syndrome with transaminitis. **(A)** Coronal MIP MRCP image shows diffuse irregularity of the intrahepatic biliary tree with a beaded appearance (arrow). **(B)** Axial contrast-enhanced T1-weighted fat-suppressed MR image shows wedge-shaped areas of arterial phase hyperenhancement (short arrow) surrounding a dilated right intrahepatic duct (long arrow). PSC with acute inflammation could have a similar appearance, but the clinical history helps to distinguish these entities.

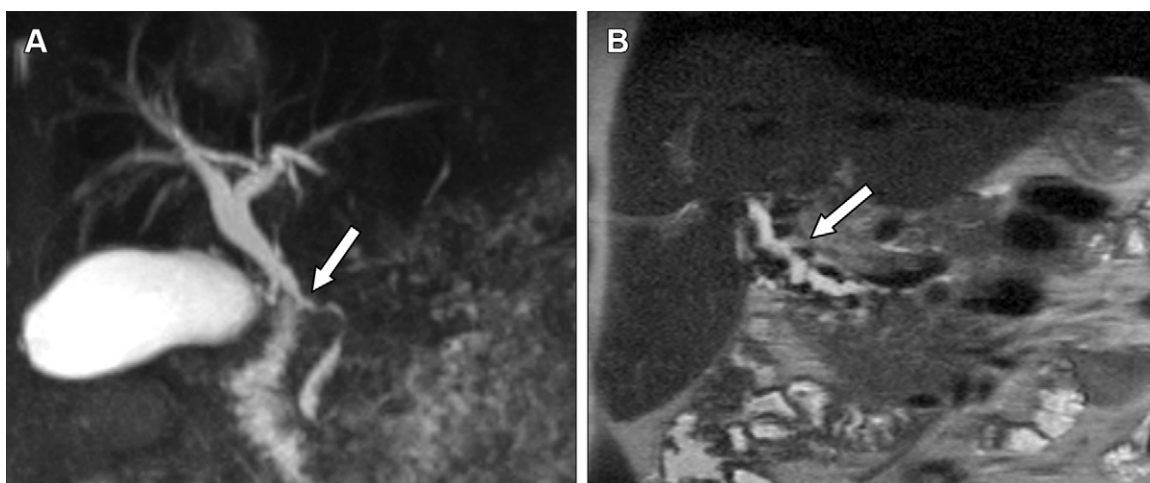


Figure 20. Portal cholangiopathy in a 43-year-old man with history of a chronic portal vein thrombus after undergoing splenectomy. **(A)** Coronal MIP MRCP image shows smooth narrowing of the common duct with a scalloped appearance (arrow). **(B)** Coronal T2-weighted MR image shows smooth, undulating external compression of the extrahepatic duct by adjacent varices, which appear as dark flow voids (arrow), compatible with varicoid-type portal cholangiopathy.

(Fig 20) and is potentially reversible (66). This type can mimic cholangiocarcinoma spreading along the duct and is sometimes called *pseudocholangiocarcinoma* (65). The fibrotic form results from ischemia due to a portal vein thrombus, causing smooth, localized strictures with progressively enhancing, thickened common bile duct walls and associated biliary dilatation. The strictures represent scarring from chronic ischemic inflammation and may not improve after venous collateral decompression (66). This form can affect intrahepatic ducts in addition to the extrahepatic ducts, and recognition of the associated vascular changes is key to determining the correct diagnosis. The mixed form combines features of the varicoid and fibrotic types, demonstrating irregular bile duct contours with multiple areas of stricture and dilatation (65). Associated biliary stasis predisposes patients to biliary stones (65).

Ischemic Cholangiopathy

Bile ducts are solely vascularly supplied by hepatic arteries via the peribiliary arterial plexus. Compromise in arteri-

al perfusion due to luminal obstruction or altered flow can result in ischemia, stricture, and occasional necrosis of bile ducts (67,68). The causes include arterial complications of a liver transplant, other hepatobiliary surgeries, or transarterial interventions. The perfusional insult can be due to large artery stenosis or occlusion or microangiopathy secondary to inflammation and rejection. Radiologic findings include single or multiple short-segment nonanastomotic biliary strictures with associated ductal dilatation (Fig S7), and occasionally, bilomas (69,70).

Ischemic cholangiopathy after a liver transplant has been classified into four patterns with distinct radiologic and clinical features: (a) diffuse necrosis, (b) multifocal progressive, (c) confluence dominant, and (d) the minor form. Diffuse necrosis shows severe radiologic changes involving most of the biliary tree. Patients with the multifocal progressive pattern demonstrate stenoses of the second order and peripheral ducts that worsen over time. Patients with these two forms commonly require retransplant. Patients with the confluence

Table 4: Pitfalls at MRI Evaluation of the Biliary System

| Pitfall or Artifact | Cause | Significance | Clues to Diagnosis |
|--|--|---|--|
| Respiratory motion artifacts | Irregular diaphragmatic excursion with subsequent suboptimal triggering during breathing-averaged acquisitions | Misregistration of the bile ducts, which can appear stenotic, discontinuous, or duplicated | Motion artifacts elsewhere on the images |
| Pulsation or “crossing vessel” artifact (Fig 24) | Vessels adjacent to the extrahepatic duct (usually right hepatic artery as it crosses the posterior aspect of the extrahepatic duct) | May simulate short-segment stricture or a filling defect on MRCP images, especially on MIP images | Absence of upstream ductal dilation; correlation with the course of the vessel on images from other sequences |
| Susceptibility artifacts | Signal intensity loss or distortion associated with surgical clips, metallic stents, pneumobilia, or bowel gas, especially during gradient-echo sequences (blooming) | May conceal abnormality or result in pseudolesions | Review of the fast spin-echo sequences, which are less sensitive to susceptibility |
| Hepatobiliary contrast gadoxetate | Shortened T2 of excreted gadolinium in bile, reducing the T2 signal intensity of bile and ducts on images from delayed sequences | Apparent intraductal filling defects on T2-weighted MR images or poor visualization of the ducts | T2-weighted MRCP sequences should be performed before hepatobiliary contrast injection |
| Flow artifact (Fig 22) | Flow of bile causes T2 hypointensity, often in the common duct just beyond the cystic duct insertion | Apparent filling defect on thin-section axial T2-weighted images may mimic choledocholithiasis | Recognize characteristic appearance in center of the duct rather than dependent location; check thicker sections and coronal sequence; hypointensity is absent on steady-state free-precession MR images, if obtained, although not required for confirming flow artifact |
| Pneumobilia (Fig S8) | Air in bile ducts appears as T2 hypointensity | May mimic bile duct stones | Recognize antidependent location of air, unlike dependent location of stones; evaluate in- and opposed-phase MR images for susceptibility artifact associated with air |
| Small filling defects obscured on MIP MRCP images (Fig 21) | Volume averaging from MIP | Small stones or filling defects may not be visible on MIP MR images | Assess source MRCP images and thin-section T2-weighted MR images for filling defects |
| Intraductal mass mimicking a stone (Figs 23, S9) | Papillary neoplasm within the duct lumen | May mimic a bile duct stone | T2 signal intensity may be higher in the mass than that in typical stones; correlate with postcontrast images for mass enhancement and diffusion-weighted MR images for restricted diffusion |
| Duodenal diverticulum | Variable duodenal diverticulum contents: fluid, gas, contrast material, debris | May mimic a biliary or pancreatic cystic lesion | Recognize air-fluid level, susceptibility artifacts, communication with bowel, characteristic location near ampulla, along medial second or superior third portion of the duodenum; negative oral contrast material may help to fill diverticulum; correlate with prior CT, if available |

Sources.—References 72, 73.

dominant pattern display strictures and casts restricted to the biliary confluence, often requiring biliary stenting but infrequently needing a retransplant. Patients with the minor form show mild radiologic abnormalities without progression, usually not needing procedural intervention (71).

Approach to Biliary Abnormalities

Pathologic conditions of the biliary tract may be seen at imaging as luminal dilatation or narrowing, filling defects within the bile ducts, wall thickening, a frank mass involving the

bile ducts, or a combination thereof. MRI and MRCP usually provide the most complete noninvasive imaging evaluation of these abnormalities but can be prone to artifacts and other pitfalls that may mimic abnormalities (Table 4) (72,73).

Although incidental biliary dilatation can be seen in a variety of clinical settings (especially after cholecystectomy), the presence of elevated alkaline phosphatase and conjugated bilirubin or new biliary dilatation suggests cholestasis and increases suspicion for an obstructive pathologic condition (3). If a true biliary abnormality is suspected and obstructing

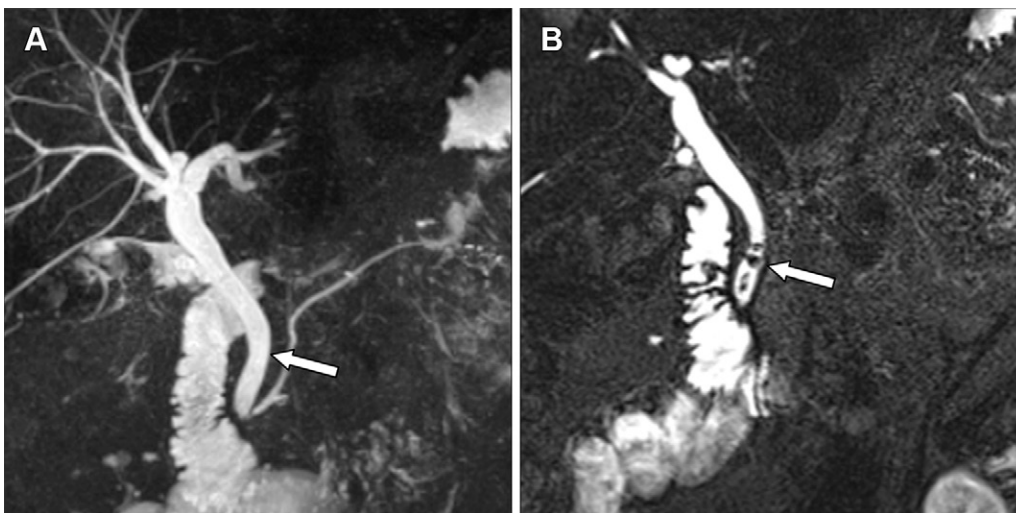


Figure 21. Choledocholithiasis in a 61-year-old man with acute pancreatitis. **(A)** Coronal MIP MRCP image shows no appreciable filling defect in the distal common bile duct (arrow). **(B)** Coronal three-dimensional MRCP source image, however, clearly shows multiple filling defects in the distal common bile duct (arrow), highlighting the importance of examining MRCP three-dimensional source images and other T2-weighted MR images for biliary filling defects.

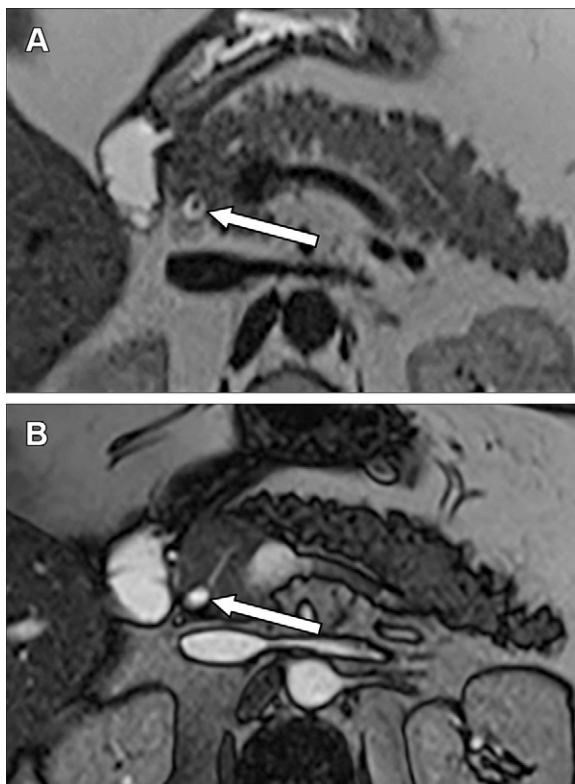


Figure 22. Flow artifact mimicking choledocholithiasis. **(A)** Axial thin-section T2-weighted MR image shows an apparent filling defect in the center of the common bile duct (arrow), a typical appearance for flow artifact but also similar to a stone in the duct. **(B)** Steady-state free-precession MR image (arrow) shows an absence of filling defect and is less susceptible to flow artifact, helping to confirm the artifact.

stones and mass lesions have been excluded, other causes of abnormal biliary morphology must be sought. Choledochal cysts should be considered when unequivocal dilatation is encountered without any obstructing cause identified at imaging, especially if an abnormal pancreaticobiliary junction or characteristic features are present (eg, the central dot sign in Caroli disease or typical morphology with an abrupt

transition to a normal caliber upstream from the dilatation). Ductal dilatation can also be the dominant imaging feature in IPNB. Scrutinizing multiple sequences including postcontrast arterial phase and diffusion-weighted MR images may help to identify an associated small solid mass, although cholangioscopy may be required for identification of the solid component. If no cause of obstruction is seen at imaging but clinical and radiologic features remain concerning for true obstruction, ERCP and/or endoscopic US is likely appropriate to evaluate for mucin or a small papillary lesion in the case of IPNB, or other imaging-occult lesions (3).

The most common biliary filling defects are stones. These show characteristic features on US images when detected, can be challenging to diagnose on CT images (although dual-energy CT can help), and are more completely evaluated with MRI. Although MRCP is the ideal imaging modality for choledocholithiasis, it is important to not rely solely on the maximum intensity projection (MIP) images, which can obscure small filling defects, but to assess the source and thin-section T2-weighted MR images for stones (Fig 21). Flow artifact from bile appears as intraductal T2 hypointensity and can mimic stones, especially on thin axial single-shot fast spin-echo MR images, but its central nondependent location distinguishes it from a stone (Fig 22) (73). Pneumobilia is also T2 hypointense and can mimic biliary stones, but it is antidependent, sometimes with an air-fluid level (Fig S8). Extensive pneumobilia reduces MRCP sensitivity for stones. Filling defects that are less T2 hypointense or larger than typical biliary stones raise concern for an intraductal soft-tissue neoplasm such as IPNB or cholangiocarcinoma and warrant scrutiny of diffusion-weighted and contrast-enhanced MRI sequences (Figs 23, S9). Intraductal cholangiocarcinomas often develop as malignant transformation of IPNBs, and the invasive component may be evident as bile duct wall disruption with mass-like infiltration of the adjacent parenchyma. Overall, cholangiocarcinoma has protean manifestations as a polypoid or intraductal, periductal, or masslike lesion, and careful evaluation is required to detect and accurately stage the lesion.

When bile duct luminal narrowing or wall thickening and enhancement are encountered, benign and malignant causes

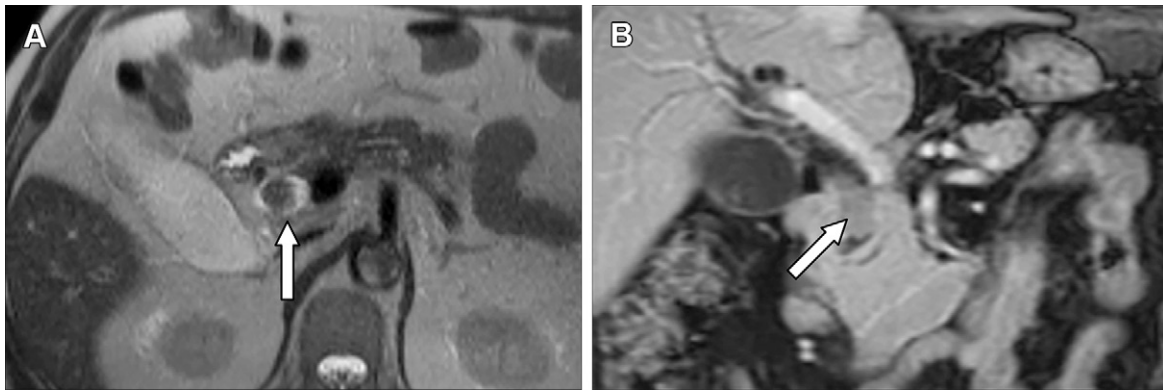


Figure 23. Distal cholangiocarcinoma with an intraductal papillary growth pattern in a 67-year-old man with a history of painless jaundice and abnormal liver function test results. **(A)** Axial T2-weighted MR image shows a round filling defect in the common bile duct that mimics a stone but is larger and, although hypointense, slightly higher in signal intensity than a typical stone (arrow). **(B)** Coronal contrast-enhanced T1-weighted fat-suppressed MR image shows enhancement of the lesion, demonstrating that it is a soft-tissue mass rather than a stone (arrow).

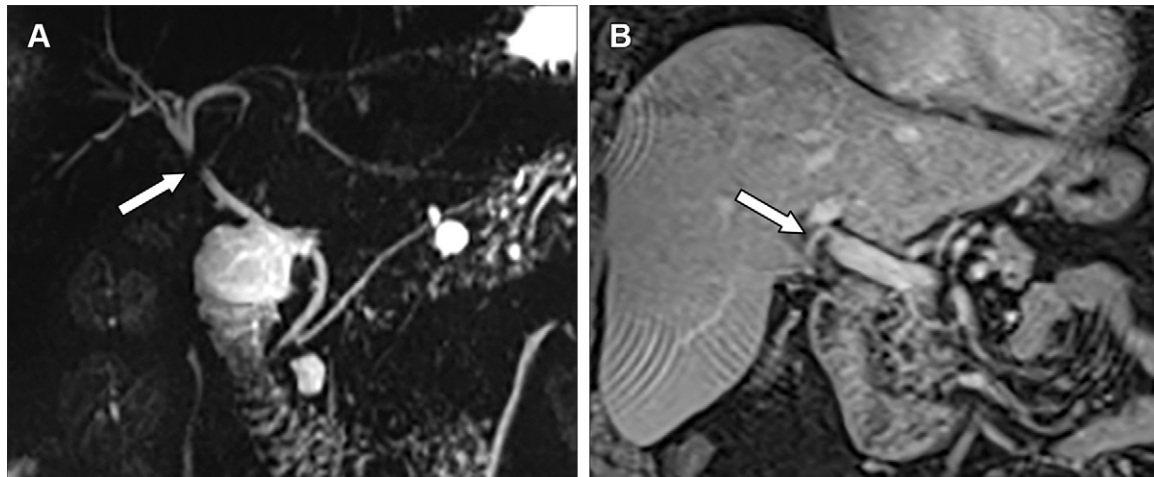


Figure 24. Crossing vessel artifact mimicking a biliary stricture in a 62-year-old woman. **(A)** Coronal MIP MRCP image shows a focal hypointense filling defect at the extrahepatic duct (arrow). Note the lack of upstream intrahepatic biliary dilatation. **(B)** Coronal contrast-enhanced T1-weighted fat-suppressed MR image shows that the hepatic artery crosses the duct at this level (arrow), confirming that vessel pulsation artifact accounts for the appearance on the MRCP image.

of stricture should be considered. Pulsation artifact from the right hepatic artery crossing posterior to the common duct should not be confused for a stricture on MRCP images. The artifact is identifiable by its characteristic location, absence of upstream biliary dilatation, and visualization of the vessel on images from other sequences (Fig 24). However, if biliary wall enhancement and upstream dilatation are present, it is important to consider a true stricture over an artifact from a crossing vessel (Fig S10). Benign biliary strictures often demonstrate circumferential duct narrowing, multiplicity, smooth margins, and a gradual transition to a normal-caliber duct. Benign strictures have a variety of causes, including previous biliary procedures, pancreatitis, infectious cholangitis, or sclerosing cholangitis. In some cases, characteristic imaging features accompanied by clinical findings may allow a specific diagnosis (Fig 25) (27,31,59,74,75). In comparison to benign strictures, malignant strictures often demonstrate irregular luminal narrowing with an abrupt transition in

caliber and shouldered edges. Asymmetric ductal wall thickening, especially that greater than 3 mm, is suggestive of malignant stricture (Figs 26, S11) (76,77). Malignant strictures are often solitary and may result in greater upstream dilatation than that in benign strictures (78). When the imaging appearance of a stricture is not clearly benign or malignant, and the patient's serum CA 19-9 level is not elevated, ERCP and/or cholangioscopy may be required. When these are inconclusive, and the patient is symptomatic, surgical resection may provide the final diagnosis.

Conclusion

A wide spectrum of diseases can affect the biliary tract, including congenital, calculous, infectious, inflammatory, and neoplastic disorders. These processes may have similar clinical signs and symptoms but differ in etiopathogenesis, prognosis, and management. Knowledge of the key imaging findings is critical to accurately diagnose and appropriately

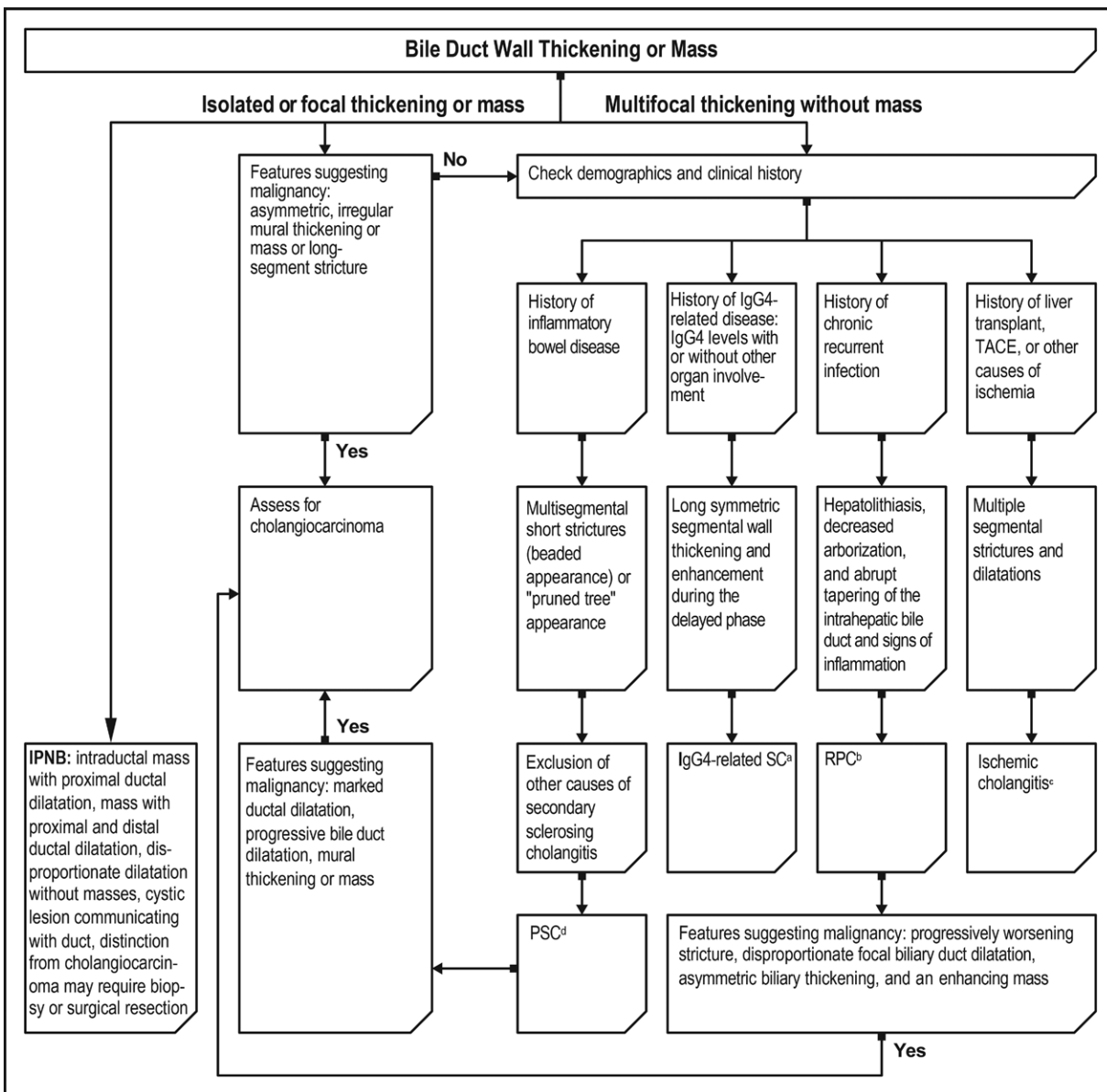


Figure 25. Flowchart shows an approach to differential diagnosis of bile duct wall thickening or a mass on the basis of demographics, clinical history, and imaging features. *RPC* = recurrent pyogenic cholangitis, *SC* = sclerosing cholangitis, *TACE* = transarterial chemoembolization. Histopathologic features include ^alymphoplasmacytic infiltration with abundant IgG4+ plasma cells, storiform interstitial fibrosis, and obliterative phlebitis; ^bbilirubinate stones and fibrous thickening of the dilated large ducts; ^cvariable depending on the degree of hepatic arterial insufficiency and the stage of disease; and ^dperiductal “onion skin” fibrosis around medium and large ducts.

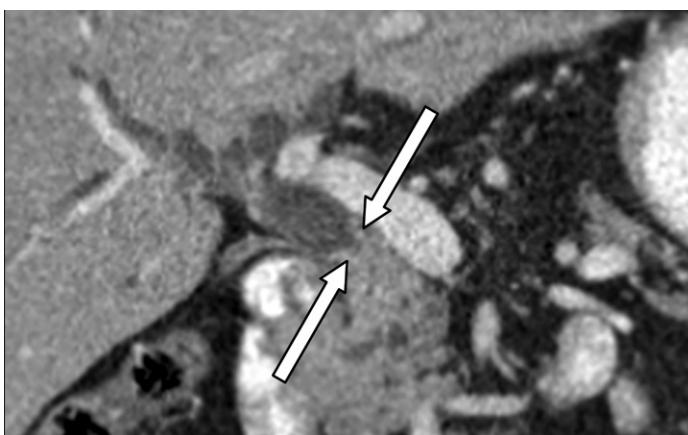


Figure 26. Malignant extrahepatic duct stricture from pancreatic cancer in a 75-year-old man. Coronal contrast-enhanced CT image shows abrupt narrowing of the extrahepatic duct (arrows) due to wall thickening greater than 3 mm, with shouldering at the margins and marked upstream biliary dilatation. These features are concerning for malignant biliary stricture. ERCP and endoscopic US demonstrated similar findings (Fig S11), and pathologic results of the mass specimen yielded pancreatic adenocarcinoma.

guide management of these disorders. Using a pattern-based approach and understanding the pearls and pitfalls of biliary imaging are essential for radiologists to assist patients and referring doctors in multidisciplinary patient treatment.

Author affiliations.—From the Departments of Radiology (C.L.V., D.L.T., A.A.B., N.A.H., H.G., H.S.R., J.M.H., L.C.K., C.G.W., P.N., F.H.M.) and Pathology (D.J.E.), Northwestern Memorial Hospital, Northwestern University Feinberg School of Medicine, 676 N St Clair St, Ste 800, Chicago, IL 60611; Department of Radiology and Imaging, Medical College of Georgia, Augusta, Ga (P.K.M.); and Department of Radiology, Mayo Clinic College of Medicine, Rochester, Minn (S.K.V.). Presented as an education exhibit at the 2022 RSNA Annual Meeting. Received June 21, 2023; revision requested August 17 and received November 8; accepted November 20. **Address correspondence to F.H.M.** (email: Frank.Müller@nm.org).

Disclosures of conflicts of interest.—The authors, editor, and reviewers have disclosed no relevant relationships.

References

- Mortelé KJ, Ros PR. Anatomic variants of the biliary tree: MR cholangiographic findings and clinical applications. *AJR Am J Roentgenol* 2001;177(2):389–394.
- Kim TU, Kim S, Lee JW, et al. Ampulla of Vater: comprehensive anatomy, MR imaging of pathologic conditions, and correlation with endoscopy. *Eur J Radiol* 2008;66(1):48–64.
- Ludwig DR, Itani M, Childs DD, et al. Biliary duct dilatation: AJR expert panel narrative review. *AJR Am J Roentgenol* 2023. 0.2214/AJR.23.29671. Published online July 26, 2023.
- Barakat MT, Banerjee S. Incidental biliary dilation in the era of the opiate epidemic: High prevalence of biliary dilation in opiate users evaluated in the Emergency Department. *World J Hepatol* 2020;12(12):1289–1298.
- Banks JS, Saigal G, D'Alonzo JM, Bastos MD, Nguyen NV. Choledochal malformations: surgical implications of radiologic findings. *AJR Am J Roentgenol* 2018;210(4):748–760.
- Katabathina VS, Kapalczynski W, Dasyam AK, Anaya-Baez V, Menias CO. Adult choledochal cysts: current update on classification, pathogenesis, and cross-sectional imaging findings. *Abdom Imaging* 2015;40(6):1971–1981.
- Al Samaraee A, Bhattacharya V. Cystic duct cyst in adults: a systematic review of the sixth entity. *Surg Today* 2023;53(5):527–543 [Published correction appears in *Surg Today* 2023;53(5):544.].
- Lee HK, Park SJ, Yi BH, Lee AL, Moon JH, Chang YW. Imaging features of adult choledochal cysts: a pictorial review. *Korean J Radiol* 2009;10(1):71–80.
- Lewis VA, Adam SZ, Nikolaidis P, et al. Imaging of choledochal cysts. *Abdom Imaging* 2015;40(6):1567–1580.
- Brown ZJ, Baghdadi A, Kamel I, Labiner HE, Hewitt DB, Pawlik TM. Diagnosis and management of choledochal cysts. *HPB (Oxford)* 2023;25(1):14–25.
- Cannella R, Giambelluca D, Diamarco M, et al. Congenital cystic lesions of the bile ducts: imaging-based diagnosis. *Curr Probl Diagn Radiol* 2020;49(4):285–293.
- Prabhakar PD, Prabhakar AM, Prabhakar HB, Sahani D. Magnetic resonance cholangiopancreatography of benign disorders of the biliary system. *Magn Reson Imaging Clin N Am* 2010;18(3):497–514, xi.
- Baron RL, Tublin ME, Peterson MS. Imaging the spectrum of biliary tract disease. *Radiol Clin North Am* 2002;40(6):1325–1354.
- Feldman MK, Coppa CP. Noninvasive imaging of the biliary tree for the interventional radiologist. *Tech Vasc Interv Radiol* 2015;18(4):184–196.
- Murphy MC, Gibney B, Gillespie C, Hynes J, Bolster F. Gallstones top to toe: what the radiologist needs to know. *Insights Imaging* 2020;11(1):13.
- Bali MA, Pezzullo M, Pace E, Morone M. Benign biliary diseases. *Eur J Radiol* 2017;93:217–228.
- Ratanaprasatporn L, Uyeda JW, Wortman JR, Richardson I, Sodickson AD. Multimodality imaging, including dual-energy CT, in the evaluation of gallbladder disease. *RadioGraphics* 2018;38(1):75–89.
- Yam BL, Siegelman ES. MR imaging of the biliary system. *Radiol Clin North Am* 2014;52(4):725–755.
- Alemi F, Seiser N, Ayloo S. Gallstone disease: cholecystitis, Mirizzi syndrome, Bouveret syndrome, gallstone ileus. *Surg Clin North Am* 2019;99(2):231–244.
- Akiyama H, Sato T, Toyoda S, Yamada H. An extrahepatic bile duct metastasis from a gallbladder cancer mimicking Mirizzi's syndrome. *Am J Gastroenterol* 1999;94(2):508–510.
- Prasad TL, Kumar A, Sikora SS, Saxena R, Kapoor VK. Mirizzi syndrome and gallbladder cancer. *J Hepatobiliary Pancreat Surg* 2006;13(4):323–326.
- Kang MJ, Jang JY, Lee KB, Han IW, Kim SW. Impact of macroscopic morphology, multifocality, and mucin secretion on survival outcome of intraductal papillary neoplasm of the bile duct. *J Gastrointest Surg* 2013;17(5):931–938.
- Katabathina VS, Flaherty EM, Dasyam AK, et al. Biliary Diseases with Pancreatic Counterparts: Cross-sectional Imaging Findings. *RadioGraphics* 2016;36(2):374–392.
- Nakanuma Y, Uesaka K, Miyayama S, Yamaguchi H, Ohtsuka M. Intraductal neoplasms of the bile duct. A new challenge to biliary tract tumor pathology. *Histol Histopathol* 2017;32(10):1001–1015.
- Nakanuma Y, Jang KT, Fukushima N, et al. A statement by the Japan-Korea expert pathologists for future clinicopathological and molecular analyses toward consensus building of intraductal papillary neoplasm of the bile duct through several opinions at the present stage. *J Hepatobiliary Pancreat Sci* 2018;25(3):181–187.
- Chatterjee A, Lopes Vendrami C, Nikolaidis P, et al. Uncommon intraluminal tumors of the gallbladder and biliary tract: spectrum of imaging appearances. *RadioGraphics* 2019;39(2):388–412.
- Zulficar M, Chatterjee D, Yoneda N, et al. Imaging features of premalignant biliary lesions and predisposing conditions with pathologic correlation. *RadioGraphics* 2022;42(5):1320–1337.
- Lee SS, Kim MH, Lee SK, et al. Clinicopathologic review of 58 patients with biliary papillomatosis. *Cancer* 2004;100(4):783–793.
- Liu LN, Xu HX, Zheng SG, et al. Ultrasound Findings of Intraductal Papillary Neoplasm in Bile Duct and the Added Value of Contrast-Enhanced Ultrasound. *Ultraschall Med* 2015;36(6):594–602.
- Park HJ, Kim SY, Kim HJ, et al. Intraductal papillary neoplasm of the bile duct: clinical, imaging, and pathologic features. *AJR Am J Roentgenol* 2018;211(1):67–75.
- Khoshpouri P, Habibabadi RR, Hazhirkarzar B, et al. Imaging features of primary sclerosing cholangitis: from diagnosis to liver transplant follow-up. *RadioGraphics* 2019;39(7):1938–1964.
- WHO classification of digestive system tumours. WHO Classification of Tumours Editorial Board. WHO classification of tumours, 5th ed. World Health Organization, 2019.
- Chung T, Park YN. Up-to-date pathologic classification and molecular characteristics of intrahepatic cholangiocarcinoma. *Front Med (Lausanne)* 2022;9:857140.
- Kirstein MM, Vogel A. Epidemiology and risk factors of cholangiocarcinoma. *Visc Med* 2016;32(6):395–400.
- Sia D, Villanueva A, Friedman SL, Llovet JM. Liver cancer cell of origin, molecular class, and effects on patient prognosis. *Gastroenterology* 2017;152(4):745–761.
- Khan SA, Tavolari S, Brandi G. Cholangiocarcinoma: Epidemiology and risk factors. *Liver Int* 2019;39(Suppl 1):19–31.
- Kendall T, Verheij J, Gaudio E, et al. Anatomical, histomorphological and molecular classification of cholangiocarcinoma. *Liver Int* 2019;39(S1 Suppl 1):7–18.
- Liau JY, Tsai JH, Yuan RH, Chang CN, Lee HJ, Jeng YM. Morphological subclassification of intrahepatic cholangiocarcinoma: etiological, clinicopathological, and molecular features. *Mod Pathol* 2014;27(8):1163–1173.
- Singhi AD, Nikiforova MN, Chennat J, et al. Integrating next-generation sequencing to endoscopic retrograde cholangiopancreatography (ERCP)-obtained biliary specimens improves the detection and management of patients with malignant bile duct strictures. *Gut* 2020;69(1):52–61.
- Chung YE, Kim MJ, Park YN, et al. Varying appearances of cholangiocarcinoma: radiologic-pathologic correlation. *RadioGraphics* 2009;29(3):683–700.
- Lee Y, Yoo IR, Boo SH, Kim H, Park HL, Hyun O J. The role of F-18 FDG PET/CT in intrahepatic cholangiocarcinoma. *Nucl Med Mol Imaging* 2017;51(1):69–78.
- DeOliveira ML, Cunningham SC, Cameron JL, et al. Cholangiocarcinoma: thirty-one-year experience with 564 patients at a single institution. *Ann Surg* 2007;245(5):755–762.
- Bismuth H, Corlette MB. Intrahepatic cholangioenteric anastomosis in carcinoma of the hilus of the liver. *Surg Gynecol Obstet* 1975;140(2):170–178.
- Jarnagin WR, Fong Y, DeMatteo RP, et al. Staging, resectability, and outcome in 225 patients with hilar cholangiocarcinoma. *Ann Surg* 2001;234(4):507–519.
- Kim DW, Kim SY, Yoo C, Hwang DW. Update on biliary cancer imaging. *Radiol Clin North Am* 2022;60(5):825–842.
- Lee DH, Kim B, Lee ES, et al; Korean Society of Abdominal Radiology. Radiologic Evaluation and Structured Reporting Form for Extrahepatic Bile Duct Cancer: 2019 Consensus Recommendations from the Korean Soci-

- ety of Abdominal Radiology. *Korean J Radiol* 2021;22(1):41–62.
47. Menias CO, Surabhi VR, Prasad SR, Wang HL, Narra VR, Chintapalli KN. Mimics of cholangiocarcinoma: spectrum of disease. *RadioGraphics* 2008;28(4):1115–1129.
 48. Sulzer JK, Ocuin LM. Cholangitis: causes, diagnosis, and management. *Surg Clin North Am* 2019;99(2):175–184.
 49. Catalano OA, Sahani DV, Forcione DG, et al. Biliary infections: spectrum of imaging findings and management. *RadioGraphics* 2009;29(7):2059–2080.
 50. O'Connor OJ, O'Neill S, Maher MM. Imaging of biliary tract disease. *AJR Am J Roentgenol* 2011;197(4):W551–W558.
 51. Kwan KEL, Shelat VG, Tan CH. Recurrent pyogenic cholangitis: a review of imaging findings and clinical management. *Abdom Radiol (NY)* 2017;42(1):46–56.
 52. Heffernan EJ, Geoghegan T, Munk PL, Ho SG, Harris AC. Recurrent pyogenic cholangitis: from imaging to intervention. *AJR Am J Roentgenol* 2009;192(1):W28–W35.
 53. Venkatesh SK, Welle CL, Miller FH, et al; IPSCSG. Reporting standards for primary sclerosing cholangitis using MRI and MR cholangiopancreatography: guidelines from MR Working Group of the International Primary Sclerosing Cholangitis Study Group. *Eur Radiol* 2022;32(2):923–937 [Published correction appears in *Eur Radiol* 2022;32(4):2860.]
 54. Morgan MA, Khot R, Sundaram KM, et al. Primary sclerosing cholangitis: review for radiologists. *Abdom Radiol (NY)* 2023;48(1):136–150.
 55. Mittal PK, Moreno CC, Kalb B, et al. Primary biliary tract malignancies: MRI spectrum and mimics with histopathological correlation. *Abdom Imaging* 2015;40(6):1520–1557.
 56. Burak K, Angulo P, Pasha TM, Egan K, Petz J, Lindor KD. Incidence and risk factors for cholangiocarcinoma in primary sclerosing cholangitis. *Am J Gastroenterol* 2004;99(3):523–526.
 57. Fung BM, Tabibian JH. Primary sclerosing cholangitis-associated cholangiocarcinoma: special considerations and best practices. *Expert Rev Gastroenterol Hepatol* 2021;15(5):487–496.
 58. Razumilava N, Gores GJ, Lindor KD. Cancer surveillance in patients with primary sclerosing cholangitis. *Hepatology* 2011;54(5):1842–1852.
 59. Tanaka A. IgG4-related sclerosing cholangitis and primary sclerosing cholangitis. *Gut Liver* 2019;13(3):300–307.
 60. Madhusudhan KS, Das P, Gunjan D, Srivastava DN, Garg PK. IgG4-related sclerosing cholangitis: a clinical and imaging review. *AJR Am J Roentgenol* 2019;213(6):1221–1231.
 61. Culver EL, Barnes E. IgG4-related sclerosing cholangitis. *Clin Liver Dis (Hoboken)* 2017;10(1):9–16.
 62. Ghafoor S, Germann M, Jüngst C, Müllhaupt B, Reiner CS, Stocker D. Imaging features of COVID-19-associated secondary sclerosing cholangitis on magnetic resonance cholangiopancreatography: a retrospective analysis. *Insights Imaging* 2022;13(1):128.
 63. Du M, Yang S, Liu M, Liu J. COVID-19 and liver dysfunction: Epidemiology, association and potential mechanisms. *Clin Res Hepatol Gastroenterol* 2022;46(2):101793.
 64. Walser EM, Runyan BR, Heckman MG, et al. Extrahepatic portal biliopathy: proposed etiology on the basis of anatomic and clinical features. *Radiology* 2011;258(1):146–153.
 65. Besa C, Cruz JP, Huete A, Cruz F. Portal biliopathy: a multitechnique imaging approach. *Abdom Imaging* 2012;37(1):83–90.
 66. Shin SM, Kim S, Lee JW, et al. Biliary abnormalities associated with portal biliopathy: evaluation on MR cholangiography. *AJR Am J Roentgenol* 2007;188(4):W341–W347.
 67. Gorla O, Archambeaud I, Lemaitre C, et al. Ischemic cholangiopathy: An update. *Clin Res Hepatol Gastroenterol* 2020;44(4):486–490.
 68. Nakanuma Y, Miyata N. Vascular supply of the bile duct and ischemic cholangiopathy. In: Nakanuma Y, ed. *Pathology of the bile duct*. Singapore: Springer, 2017; 55–70.
 69. Giesbrandt KJ, Bulatao IG, Keaveny AP, Nguyen JH, Paz-Fumagalli R, Taner CB. Radiologic characterization of ischemic cholangiopathy in donation-after-cardiac-death liver transplants and correlation with clinical outcomes. *AJR Am J Roentgenol* 2015;205(5):976–984.
 70. Alabdulghani F, Healy GM, Cantwell CP. Radiological findings in ischemic cholangiopathy. *Clin Radiol* 2020;75(3):161–168.
 71. Croome KP, Mathur AK, Aqel B, et al. Classification of distinct patterns of ischemic cholangiopathy following DCD liver transplantation: distinct clinical courses and long-term outcomes from a multicenter cohort. *Transplantation* 2022;106(6):1206–1214.
 72. Itani M, Lalwani N, Anderson MA, Arif-Tiwari H, Paspulati RM, Shetty AS. Magnetic resonance cholangiopancreatography: pitfalls in interpretation. *Abdom Radiol (NY)* 2023;48(1):91–105.
 73. Welle CL, Miller FH, Yeh BM. Advances in MR imaging of the biliary tract. *Magn Reson Imaging Clin N Am* 2020;28(3):341–352.
 74. Seo N, Kim SY, Lee SS, et al. Sclerosing cholangitis: clinicopathologic features, imaging spectrum, and systemic approach to differential diagnosis. *Korean J Radiol* 2016;17(1):25–38.
 75. Sundaram KM, Morgan MA, Itani M, Thompson W. Imaging of benign biliary pathologies. *Abdom Radiol (NY)* 2023;48(1):106–126.
 76. Katabathina VS, Dasyam AK, Dasyam N, Hosseinzadeh K. Adult bile duct strictures: role of MR imaging and MR cholangiopancreatography in characterization. *RadioGraphics* 2014;34(3):565–586.
 77. Kim JY, Lee JM, Han JK, et al. Contrast-enhanced MRI combined with MR cholangiopancreatography for the evaluation of patients with biliary strictures: differentiation of malignant from benign bile duct strictures. *J Magn Reson Imaging* 2007;26(2):304–312.
 78. Sonavane SK, Menias CO. Imaging biliary strictures: a pictorial review. *Curr Probl Diagn Radiol* 2014;43(1):14–34.